STUDIES OF THE FREQUENCY DEPENDENCE OF THE MICROWAVE SURFACE RESISTANCE OF HIGH T_C SUPERCONDUCTING FILMS USING A NEW SUPERCONDUCTING SPLIT RING RESONATOR

By

Bruce T. Gowe

B. Sc. (Physics) University of British Columbia

A THESIS SUBMITTED IN PARTIAL FULFILLMENT OF

THE REQUIREMENTS FOR THE DEGREE OF

MASTER OF SCIENCE

in

THE FACULTY OF GRADUATE STUDIES

DEPARTMENT OF PHYSICS AND ASTRONOMY

We accept this thesis as conforming

to the required standard

THE UNIVERSITY OF BRITISH COLUMBIA

September 1997

In presenting this thesis in partial fulfilment of the requirements for an advanced degree at the University of British Columbia, I agree that the Library shall make it freely available for reference and study. I further agree that permission for extensive copying of this thesis for scholarly purposes may be granted by the head of my department or by his or her representatives. It is understood that copying or publication of this thesis for financial gain shall not be allowed without my written permission.

Department of Physics and Astronomy
The University of British Columbia
2075 Wesbrook Place
Vancouver, Canada
V6T 1W5

Date: October 14, 1997

Abstract

A new superconducting split-ring resonator has been developed for use in perturbation measurements of the microwave surface resistance of thin superconducting films. The experimental setup allowed for the sample temperature to be ramped from 10 – 120 K during the measurement. The split ring arrangement was such that it could be adjusted from run to run to operate at a variety of frequencies thus making the apparatus well suited to exploring the frequency dependence of the film's losses. Results from measurements on $Tl_2Ba_2CaCu_2O_y$ films with this resonator at 910 MHz, 1.4 GHz and 2.4 GHz in conjunction with results from an earlier split-ring resonator at 3.7 GHz [1] suggest that the losses are not consistent with an ω^2 relationship below 2.4 GHz. Operating at 910 MHz, surface resistances as low as $5\mu\Omega$ were easily resolved with perturbations from an unloaded quality factor of $2x10^6$. The 2.4 GHz configuration had a resolution of $1\mu\Omega$ in surface resistance.

Table of Contents

List of Tables

List of Figures

Acknowledgement

There are many people who are deserving of thanks for the help, guidance, and inspiration that they have provided me throughout the time of my work on this research project. Their contributions have taken the form of overt help when asked and of fine modeling of character.

To begin with, I would like to thank Doug Bonn, my research supervisor. In addition to Doug's technical expertise and extensive knowledge of his field, his passion for Physics in general has made this work a very enjoyable experience for me. Thanks also to Walter Hardy who has also answered many of my questions and always been a fine example of character to follow.

Many thanks also to other members of the lab including Pinder Dosanjh for his technical help and Amhad Hosseinni for his help with the development of the time domain measurements. Also a huge thank you is in order for Saeid Kamal. In addition to always delivering with a smile all of the answers to every problem or question that arose, his development of the control software has been indispensible.

Thanks are also deserved by members of the machine shop, specifically to George Babinger for all of his valuable assistance in the student shop and to Phil Akers who machined the final version of the resonator.

I would also like to thank the many students and staff members of Penticton High School who have helped encourage me to return to UBC for my Masters.

A very special thanks goes to my family for their support. My wife, Shaune, has encouraged and supported me with her love throughout my research.

Finally, thanks must also go to STI of Santa Barbara California for providing the low

loss high-T_c $Tl_2Ba_2CaCu_2O_y$ samples.

This work was funded by STI, CIAR, and NSERC.

Chapter 1

Introduction

1.1 Introduction to High Tc Surface Resistance

The search for low loss conductors is common to many fields of physics and engineering such as band pass filters, particle accelerators and high field electromagnets. Many of the DC applications were revolutionized by the discovery of superconductivity by Kammerling-Onnes in 1911. Electromagnets operating above 2 Tesla in MRI applications can now be run indefinitely without the need for electrical power through the use of Nb:Ti wire which undergoes a superconducting transition at 10 K. For the AC applications, however, the situation is not as simple or ideal, with both normal metals and superconducting materials showing joule losses. Nevertheless, with the lower losses available with the use of superconductors, it is now possible to build filters[2] with sharper roll off's and accelerating cavities that require less RF power to maintain the desired internal electric fields.

In the case of oscillating electric and magnetic fields applied to the surface of a conductor, the quality of the conductor is usually described in terms of the surface resistance R_s , which is the real part of the surface impedance Z_s .

$$R_S = \mathrm{Re}\,(\,Z_S\,) \tag{1.1}$$

For good conductors and type II superconductors, the derivation of the relationship between R_s and the conductivity is as follows. One begins with a time varying magnetic

field applied in the "z" direction which is tangent to the surface of the material which occupies the half space $x > 0$. With the additional assumption of local electrodynamics (usually appropriate for type II superconductors) we have,

$$\mathbf{H} = \mathrm{H}_0\, e^{i\omega t}\, \hat{\mathbf{z}} \qquad , \qquad \mathrm{J} = \sigma \mathrm{E} \tag{1.2}$$

where σ is the complex conductivity.

From the curl of the second Maxwell equation we have,

$$\nabla \times (\nabla \times \mathbf{H}) = \nabla \times \mathbf{J} + \epsilon_0 \frac{\partial}{\partial t}(\nabla \times \mathbf{E}) \tag{1.3}$$

which, with the Maxwell equations, $\nabla \cdot \mathbf{B} = 0$, and $\nabla \times \mathbf{E} = -\frac{\partial \mathbf{B}}{\partial t}$, can be written,

$$-\nabla^2 \mathbf{H} = \nabla \times \mathbf{J} - \epsilon_0 \mu_0 \frac{\partial^2}{\partial t^2} \mathbf{H}\,. \tag{1.4}$$

Adding the conditions of equation 1.2, equation 1.4 becomes,

$$\frac{\partial^2 \mathrm{H_z}}{\partial x^2} = i\, \mu_0 \omega \sigma\, \mathrm{H_z} - \epsilon_0 \mu_0 \omega^2\, \mathrm{H_z}\,. \tag{1.5}$$

The ω^2 term can be ignored if the condition,

$$2\pi\, \epsilon_0\, f << |\sigma| \tag{1.6}$$

is satisfied. For frequencies as high as 3.7 GHz, this requires that the resistivity meet the condition $\rho << 70(\Omega m)$ ($\rho = [\mathrm{Re}(\sigma)]^{-1}$) which is easily satisfied for even lead at room temperature ($\rho_{lead} = 2 \times 10^{-3} \Omega m$). Solving equation 1.5 then gives the normal component of the H field within the conductor,

$$\mathrm{H_z} = \mathrm{H_0\, e^{-kx}} \qquad , \qquad \mathrm{k} = (\mathrm{i}\, \mu\omega\sigma)^{1/2} \tag{1.7}$$

The surface impedance Z_S is defined as the ratio of tangential electric and magnetic fields at the surface,

$$Z_S = \frac{\mathrm{E_{0y}}}{\mathrm{H_{0z}}} \tag{1.8}$$

and from the Maxwell equations, the electric field at the surface can be written in terms of the magnetic field via,

$$\mathrm{E_{0y}} = \left(\frac{i\,\mu_0\omega}{k}\right)\,\mathrm{H_{0z}} \tag{1.9}$$

Substituting into equation 1.8 then gives the general form of Z_S for both normal metals and superconductors.

$$Z_S = \left(\frac{i\,\mu_0\omega}{k}\right) = \left(\frac{i\mu_0\omega}{\sigma}\right)^{1/2} = R_S + i\,X_S \tag{1.10}$$

For a metal, the conductivity σ is real and equations 1.7 and 1.10 respectively become,

$$k^{-1} = \left(\frac{2}{\mu_0\omega\sigma}\right)^{1/2}\frac{(1-i)}{2} \tag{1.11}$$

$$Z_{S(metal)} = (1+i)\left(\frac{\mu_0\omega}{2\sigma}\right)^{1/2} \tag{1.12}$$

Equation 1.11 can be written in terms of the well known "skin depth" $\delta = (\frac{2}{\mu\omega\sigma})^{1/2}$ for the complex propagation of RF fields into a normal metal. Thus the surface resistance R_S, being the real part of Z_S, is then simply given by,

$$\mathrm{R_{s(metal)}} = \left(\frac{\mu_0\omega}{2\sigma}\right)^{1/2} \tag{1.13}$$

It is therefore apparent that for applications involving normal metals, the conducting surfaces will produce losses with an $\sqrt{\omega}$ frequency dependence.

For a superconductor, on the other hand, the conductivity becomes complex due to the "two fluid" nature of the carriers. The normal state fluid is governed by the usual ohmic relation,

$$J_n = \sigma_1 E \tag{1.14}$$

The superconduction fluid on the other hand is described, in the limit of local electrodynamics, by the London Equation,

$$E = \mu_0 {\lambda_L}^2 J_s \tag{1.15}$$

which accommodates the perfect DC resistivity and the screening of the Meisner Effect. λ_L is the "London Penetration Depth" and is given by

$$\lambda_L = \left(\frac{\mu n_s e^2}{m^*}\right) \tag{1.16}$$

In the case of oscillating RF fields, equation 1.15 can be written in the form,

$$J_s = \frac{-i}{\mu_0 \omega {\lambda_L}^2} E = -i\sigma_2 E \quad , \quad \sigma_2 = \frac{1}{\mu_0 \omega {\lambda_L}^2} \tag{1.17}$$

Thus including both contributions to the conductivity, the surface impedance Z_S for a type II superconductor is given exactly by

$$Z_{S(s/c)} = \left(\frac{i\mu_0\omega}{\sigma_1 - \left(\frac{i}{\mu_0\omega{\lambda_L}^2}\right)}\right)^{1/2} = \mu_0^{3/2}\omega^{3/2}{\lambda_L}^2\left(i\sigma_1 - (\mu_0\omega{\lambda_L}^2)^{-1}\right)^{1/2} \tag{1.18}$$

taking the real part of Z_S, we have,

$$R_{S(s/c)} = \frac{\mu_0^{3/2}\omega^{3/2}{\lambda_L}^2}{\sqrt{2}}\left[(\mu_0\omega{\lambda_L}^2)^{-2}\left[\left(\frac{{\sigma_1}^2}{(\mu_0\omega{\lambda_L}^2)^{-2}} + 1\right)^{1/2} - 1\right]^{1/2}\right] \tag{1.19}$$

Equation 1.19 can be simplified in the limit that the magnitude of the superfluid conductivity dominates over that of the normal fluid which is the case everywhere except very close to T_c . Then, in the limit $(\sigma_1/\sigma_2) << 1$, R_S becomes,

$$R_s = \frac{1}{2}\mu_0^2 {\sigma_1}^2 {\lambda_L}^3 \omega^2 \tag{1.20}$$

With the additional assumption that the conductivity spectrum is Drude like and the fact that $\lambda(T) \sim \lambda(0)$ (except near T_c), derivations [3] reveal a temperature dependent Surface Resistance given by,

$$R_S = \frac{\mu^2}{8\pi}\omega^2\lambda(0)(1 - x_n(T))^{-3/2}x_n(T)\frac{\tau}{1+\omega^2\tau^2} \tag{1.21}$$

where $x_n(T)$ represents the normal fluid fraction of the carriers.

Worthy of noting is the fact that, in the case of the superconductor, the surface resistance is expected to depend essentially quadratically on ω, unlike the normal metal where the dependence varies as $\sqrt{\omega}$. At first sight this may seem to suggest that for any microwave application the superconductors may be outperformed by a normal metal. Due to the small size of λ in equation 1.20, however, this is not actually the case and superconductors do offer less loss than normal metal materials.

Exploiting the lower losses that are possible when using superconducting surfaces, RF accelerating cavities have been constructed[4] out of niobium with Q factors in excess of $2x10^{11}$ at 10.5 GHz. Even using lead:tin compounds that have the advantage of being relatively stable in atmosphere, cavities have been constructed[5] that operate at frequencies of 2.85 GHz with Q factors as large as $4x10^9$. For such applications the benefits of running less RF power into the cavity outweigh the need to operate the cavity with the entire surface cooled to liquid helium temperatures. For some applications though, the cost of operating at helium temperatures is prohibitive. This is the case with passive microwave filter devices that must operate within the confines of earth orbiting satellites. It is also desirabe to avoid the use of liquid helium within the low maintenance microwave filter devices that are commercially available to cellular phone providers, as these devices need to be opeated unattended for weeks at a time.

Discovered in 1986, the family of high temperature superconducting cuprates have

drastically modified the use of superconductors in RF applications. With transition temperatures greater than that of liquid nitrogen, operation of devices incorporating these materials can now be done with greater ease and less expense compared to traditional helium cooled superconductors. In fact, some devices are calibrated with liquid nitrogen at 77 K and then operated in isolation for indefinite periods of time using closed cycle fridge systems operating at nitrogen temperatures. With the applications also comes the need for accurate methods of determining the surface resistance for the new components. Finding testing platforms for devices for use with cellular phone equipment, which operate near 1 GHz, has proven to be particularly difficult due to the size of the characteristic wavelengths involved. This challenge originates from the fact that the superconducting microwave components under test are often only cm's in size and the free space wavelength of the operating frequency, which is usually characteristic of the size of the testing apparatus, may approach 30 – 50 cm in size. In the case of high quality low loss samples, it is often difficult to resolve sample losses from losses occuring elsewhere in the testing equipment due to its relatively larger size.

1.2 Introduction to Thin Films

High temperature superconducting oxides are anisotropic in nature with Cu-O planes running in the a-b direction. The most thoroughly studied oxide is $YBa_2Cu_3O_{6.95}$ which has lattice constants of 1.93 Å and 1.96 Å in the "a" and "b" direction and a much larger 11.4 Å in the "c" direction. These materials can be produced in a variety of different forms.

Firstly, single crystals can be grown to several mm in size in the a-b direction. With no grain boundaries present, the single crystals exhibit the lowest losses in comparison to the other two forms. Although suitable for pure research purposes, few applications are

possible with the small size and large expense of the crystals. Pellets formed by pressing reacted powders represent a second form. Without the size restrictions of single crystals, ceramic like materials might be applied to hydro transmission applications where large low or zero frequency currents need to be passed along superconducting wires with thick cross sections. Unfortunately, with the large density of grain boundaries in the pellet form, they cannot be used for applications such as particle accelerators or high frequency filters because in these cases, the currents travel within the London Penetration depth and the resulting surface resistance, which is dominated by currents running across grain boundaries, is too great even though the DC conductivity is infinite.

Thin films of superconductors grown on a substrate are a third form of this material and have the most potential for use in RF applications. There are several techniques that are currently used to deposit the films onto their substrates including molecular beam epitaxy, sputtering, and laser ablation. Such techniques do allow for large patterned films to be created but it is not without a new set of difficulties. It is difficult to obtain underlying substrates that are lattice matched to the deposited superconductor, especially so when different thermal contractions and changing crystal phases are considered. Furthermore, the film growing processes do not always have complete control over the deposition stoichiometry over the entire film. Although, one has better control of the chemistry of $YBa_2Cu_3O_{6.95}$ as compared to $Tl_2Ba_2CaCu_2O_y$, with T_c 's at 93 K and 108 K respectively, the thallium compound may be preferred if one intends the applications to operate at temperatures as high as, or perhaps even slightly higher than, liquid nitrogen.

1.3 Introduction to Cavity Perturbation Measurements

With the demand of applications and the ability to grow patterned films in place, there is a need to develop a method of determining surface resistances at the frequencies of interest. As mentioned before, frequencies near 1 GHz have several significant challenges which need to be overcome.

Microwave cavity perturbation measurements have proven to be a sensitive technique for measuring R_s in both single crystals and films of high T_c superconductors. As the name suggests, cavity perturbation measurements entail perturbing a microwave cavity by exposing samples to the RF fields and recording perturbations in both the frequency f and the quality factor Q of the resonance. The fundemental definition of the Q factor is

$$Q = 2\pi \frac{(energy\ stored\ in\ the\ resonator)}{(energy\ lost\ per\ cycle)} \tag{1.22}$$

Letting E be the energy stored within the resonator and T the period of oscillation, equation 1.22 can be rewritten as

$$Q = 2\pi \frac{E}{-T \times \frac{dE}{dt}} \tag{1.23}$$

$$\frac{dE}{dt} = \frac{-2\pi f E}{Q} \tag{1.24}$$

for which the solution, expressed in terms of the decay time $\tau = Q/(2\pi f)$,

$$E = E_O e^{-t/\tau} \tag{1.25}$$

offers a convenient method of determining a resonator's Q factor.

By observing the undriven "ringing down" of the energy within the resonator, the Q is given by

$$Q = 2\pi f \tau \tag{1.26}$$

Adding the sample to the cavity both perturbs the frequency due to a slight rearrangement of the RF fields and introduces new losses to the cavity which increase the total losses per cycle thus lowering the measured Q.

Several different methods of cavity perturbation measurements are available, each differing in the way the sample is exposed to the RF fields. For situations where the wavelengths are small and the samples large enough, entire walls of a microwave cavity (one end plate in a cylindrical cavity for example) can be replaced by the material under test. In a somewhat similar fashion, dielectric resonators composed of dielectric cylinders held between two endplates[6] made from the material in question can also be used. For cases where the samples are small, single crystals for example, and the wavelengths as large as those characteristic of 1 GHz, endplate replacement is not possible. It is also difficult to examine the temperature dependence of the material under test using end plate replacement as this would entail thermally isolating the endplate. Instead, it is preferable to insert the smaller sample through a small hole into the RF fields contained within the resonator. If the hole through which the sample is inserted is small enough to be beyond the cutoff frequency, the sample can be considered out of the resonator by moving it a small distance up the hole. To some extent, the sample can be oriented in such a way as to screen the sample holder and even the underlying substrate from the RF fields found within the cavity.

As the sample is lowered into the cavity, the $\Delta(f)$ can be used to reproduce the position when similar measurements are made with a reference sample of known R_s .

The additional losses perturb the Q factor via

$$2\pi\Delta(1/Q) = \frac{(\textit{cavity losses including the sample }) \; - \; (\textit{bare cavity losses})}{(\textit{energy stored in the cavity})} \tag{1.27}$$

At the sample itself, the power dissipated into the surface is given by the time averaged normal component of the Poynting Vector,

$$|\mathrm{S_{ave}}| = \frac{\mathbf{1}}{\mathbf{2}}\,\mathrm{Real}(\mathbf{E_0} \times \mathbf{H_0^*}) \tag{1.28}$$

where E_0 is given by equation 1.9 thus giving,

$$|\mathrm{S_{ave}}| = \frac{\mathbf{1}}{\mathbf{2}}\,\mathrm{Real}(\mathrm{Z_s})\,\mathrm{H_0^2} = \frac{\mathbf{1}}{\mathbf{2}}\,\mathrm{R_s}\,\mathrm{H_0}^2 \tag{1.29}$$

Thus, the loss occurring in the superconducting sample is proportional to the square of the magnetic field at the surface of the sample. Since, for any given field pattern within the resonator, the size of H^2 near the sample is proportional to the energy stored within the resonator, the H^2 term in equation 1.29 is normalized by the "energy within the resonator" term in equation 1.27. So by combining equations 1.27 1.29, we have that

$$R_S = \beta\Delta(1/Q) \tag{1.30}$$

where the proportionality constant β can be later determined by calibrating with a known sample positioned at the same location, using information from the Δf perturbation.

Due to the reciprocal nature of the Q factor in equation 1.30, accurate measurements of the low values of R_s exhibited by the latest high quality films require that the unloaded Q factor (Q_O) be as large as possible. In fact, in its state of lowest loss, the small sample surface must present losses in the cavity that are on the same order or greater than the losses found over the remaining surface of the entire cavity. In other words, for a given

low loss sample, the cavity walls must be of sufficient quality to offer comparable or lower loss. Thus, to compete with a small superconducting sample, the walls of the cavity must have a R_s that is so low that they too must be superconducting in order to ensure that (1/Q) is sufficiently perturbed.

The use of a superconducting cavity brings in a new set of challenges. Certainly not the least of these challenges is the fact that if an elemental superconductor is used for the cavity surface it must be operated at or below liquid helium temperatures. This is challenging when one considers the fact that the information of the sample R_s is most often desired at the much higher temperature of liquid nitrogen where its application will operate. Solutions to this problem entail thermally isolating the sample from the cavity. This separation allows for the sample temperature to be ramped during the measurement of R_s while the Q_O remains essentially constant.

Even with a superconducting cavity, measurements of thin film superconducting samples that are ~5 mm in size are extremely difficult at frequencies around 1 GHz. For these frequencies, the free space wavelengths are ~30 cm with similarly sized resonant cavities. With such disparity in size, it is almost impossible to generate fields at the sample that are large enough to produce losses that are comparable to the losses found over the entire resonator surface. This lack of sufficient perturbation is the motivating factor for exploring the smaller sized split-ring resonators whose geometry (which is discussed in Chapter 2) is such that the fields can be concentrated down to a size similar to that of the sample.

Chapter 2

The New Resonator Design

All microwave measurements on the thin films were made using so called *Split-Ring* resonators. The 3.7 GHz measurements were made with an existing resonator while all other measurements were performed with the newest design, both of which are described below.

2.1 Introduction to Split-Ring Resonators

Split-Ring resonators conveniently address the rather difficult microwave frequency range for cavity perturbation measurements near 1 GHz. Although it is possible to build a cylindrical cavity that operates at 1 GHz, its diameter would be ~60 cm in size if one operates in the TE_{011} mode. Not only would this be unmanagably large for machining and handling, it would be very expensive to operate due to the large consumption of liquid helium. Admittedly, such a resonator would have a very large Q factor. At the same time, however, samples that are ~5 mm in size will not cause significant perturbation when introduced to the cavity. This is due to the fact that, in general, for a given stored energy within the resonator, $\mathbf{H} \propto D^{-1}$, where "D" is the characteristic size of the resonator. Thus, for losses at the sample, $Loss_{sample} \propto \mathbf{H}^2 \propto D^{-2}$. When comparing these sample losses to the losses occurring elsewhere on the walls of the resonator ($Loss_{walls} \propto Q^{-1} \propto D^{-1}$), one can see that the sensitivity of the measurement is inversely porportional to "D".

The split-ring resonator, unlike a cavity or $\lambda/4$ resonator, is most akin to a tuned LC

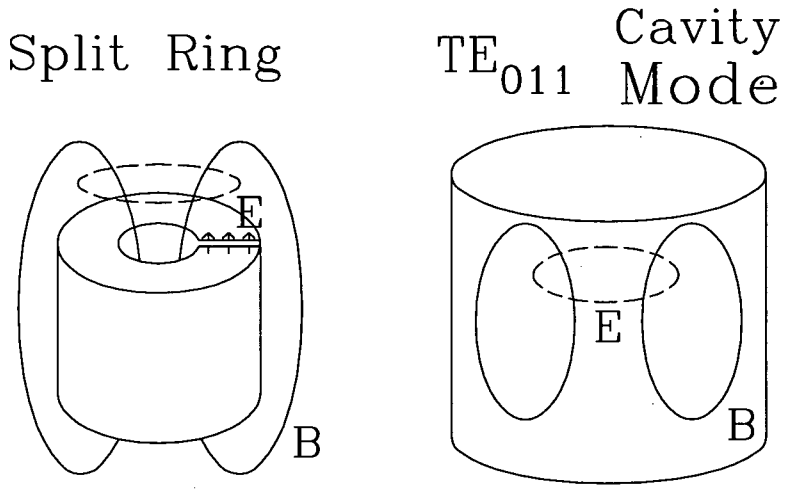

Figure 2.1: General Form of a Split Ring Resonator & a TE_{011} Cavity Mode

circuit. It is formed by cutting one or more "splits" into a metallic ring. The faces of the gap within the split act in the role of a capacitor while the ring itself behaves as a single turn inductor. Split ring resonators can also be constructed by cutting splits into dielectric material[7] but the resulting Q factors are much lower than for metals.

The resonant mode shown in figure 2.1 is similar to the TE_{011} mode in a cylindrical cavity. The TE_{011} mode is often chosen in efforts to increase the unloaded Q factor. This choice is made not only because it is intrinsically the highest Q mode of a cylindrical cavity, but also due to the fact that many cylindrical resonators are constructed with an RF joint running along the circumference of one of the end plates and the TE_{011} mode offers a field pattern that does not induce currents to cross this joint in the resonator. This benefit of the TE_{011} mode often outweighs the fact that it is not the lowest mode of a cylindrical cavity and is in fact degenerate with the TM_{111} mode, thus requiring some form of symmetry breaking within the resonator. A disadvantage of the TE_{011} cavity mode, however, is that in the case of small samples inserted down the center

line of the cavity, as is often the case in practice, the sample must be located near the centre of the cavity if one desires to reach the location where the H fields are strongest. Depending on the arrangement, this may expose parts of the sample holder (vacuum grease, for example) to the RF fields. This desire to have the sample located in the most concentrated region of H fields stems from the need to increase the sensitivity when working with low loss samples that offer little perturbation to the cavity. Indeed, even with Q factors as high as $8x10^7$ in a niobium TEM cavity[8] (which offers an order of magnitude better resolution than a TE cavity) it takes a 24mm diameter sample to induce enough loss to resolve $20\mu\Omega$'s of surface resistance. The arrangement also requires the sample to be thermally attached to the cavity thus limiting the measurement to helium temperatures at the sample.

The situation in the split-ring geometry is considerably better. Since the sample is lowered down the centerline, the ring can be designed to concentrate the H fields to a width that more closely reflects the size of the sample. For the newest split-ring resonator, the diameter of the central bore is $\sim$3 mm which is in fact smaller than that of the 4mm diameter sample film. Split-ring resonators, being small in size, are much easier to machine and handle, and are cheaper to operate.

Concentrating the fields near the sample shows up directly in the filling factor η for the perturbation arrangement where:

$$\eta = \frac{\text{magnetic energy stored in the sample area}}{\text{magnetic energy stored in the resonator}} \tag{2.31}$$

Since the losses induced in the sample are proportional to the magnetic energy stored near the sample, one wants to maximize the product of η and Q in order to maximize the sensitivity of a perturbation measurement on a low loss sample.

It is fortunate that the split-ring does have a large filling factor for it is necessary to make up for the fact that the unloaded Q factor is never as high as that of a TE_{011} mode

of similar frequency. This is due to the fact that the ratio of RF surface area (which is where the losses occur) to the RF volume is much larger for the complicated topology of the split-ring in comparison to the more simple shape of a right cylindrical cavity.

Another component of the split-ring resonator is the addition of an outer shielding tube. Operating the split-ring within a shielding tube helps to increase the Q factor by eliminating losses due to microwave fields radiating power away from the resonator. The tube diameter needs to be small enough, of course, to ensure that the operation is beyond the cutoff frequency to prevent it acting as a waveguide. The shielding tube also offers additional capacitance to the ring which has to be accounted for when the resonant frequency is calculated.

Adding dielectric material inside the gap is a further variable which can be considered at the design stage. The newest resonator uses sapphire within the gap to both lower the frequency further, through increased capacitance, and to aid in sizing the gap consistently. One must ensure than any such dielectrics used within the gap are of sufficiently low loss that they do not lower the unloaded Q of the resonator. Operating at these frequencies and Q factors, materials such as teflon would not be appropriate for this reason. Derivations of the resonant frequency have been performed[9] in the infinite length limit where the currents and electric fields are everywhere perpendicular to the axis and the magnetic fields are everywhere parallel to the axis of the split-ring. The length of the rings is chosen to be long enough to produce the desired field pattern (i.e. experimental frequencies matching reasonably well to calculated frequencies) but short enough to keep the stored energy in the resonator small compared to the losses added at the sample location during the perturbation. The new resonator rings typically are as long as they are wide.

The resonant frequency estimate by Hardy and Whitehead[9] using the labelling in figure 2.2 is given by:

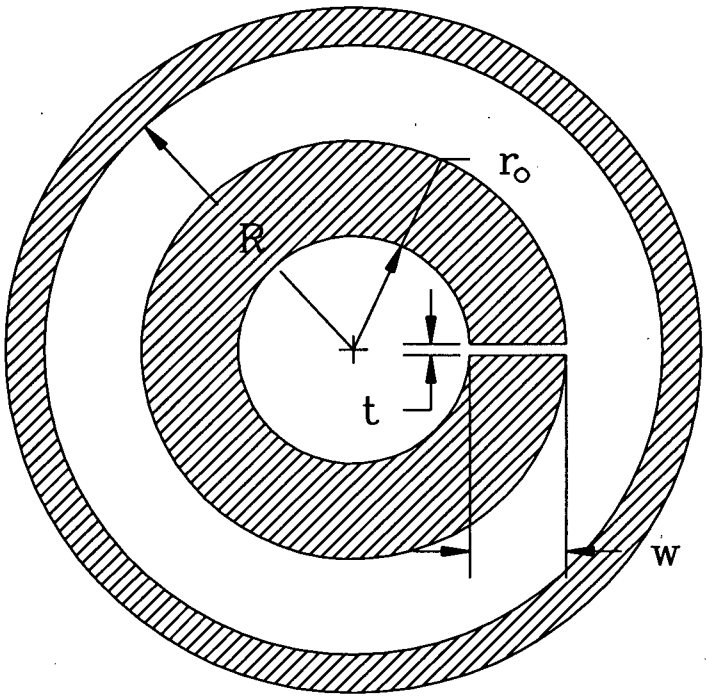

Figure 2.2: Top view of the resonator with labelling used

$$\omega_O = (1 + \frac{A_1}{A_2})^{1/2} (\frac{t}{\pi w})^{1/2} \frac{c}{r_O} \tag{2.32}$$

where:

$$A_1 = \pi r_O^2, A_2 = \pi[R^2 - (r_O + w)^2] \tag{2.33}$$

Dielectric material in the gap of the split-ring increases the capacitance of the gap and therefore effectively reduces the value of "t" by a factor equal to the dielectric constant of the material.

2.2 The 3.8 GHz Resonator

The original resonator of Bonn et al.[1] was used for the 3.7 GHz data. The ring is machined in three pieces that are screwed together to form a resonator with a single air gap. The entire resonator has been electroplated with a lead:tin compound (described below) which becomes superconducting at 7.2 K at 1 atm. Care must be taken to form good RF joints where the 3 pieces meet to prevent weak links from developing while operating in the superconducting state. These weak links occur when the currents, forced to travel across the joints through small points of contact, exceed the critical current and locally drive the surface into the normal state. Weak links do occasionally persist from run to run, requiring the resonator to be reassembled, and often to be replated as well.

The resonator is mechanically and electrically attached to the shielding tube as shown in figure 2.3. Although this connection allows for an excellent thermal link to the bath, care must be taken in such constructions so as not to create any $\lambda/4$ resonances that are close enough in frequency to the mode of the split-ring to cause extra losses due to mode coupling.

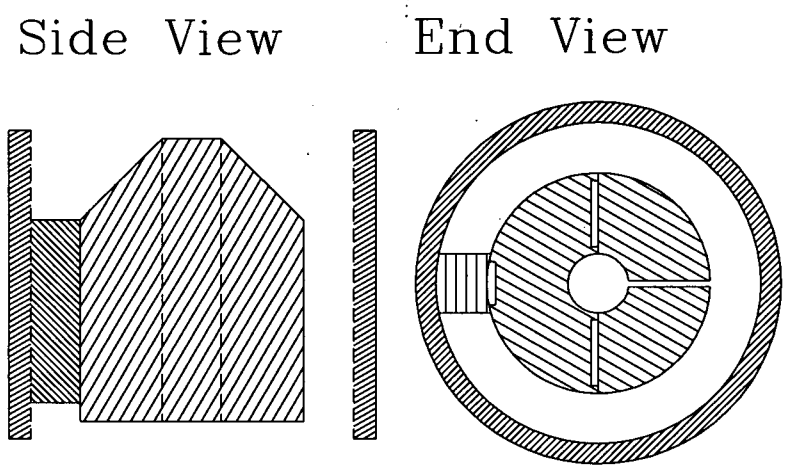

Figure 2.3: The 3.7 GHz Resonator

Transmission coupling to this resonator is achieved using two loops positioned underneath the ring assembly, one for input coupling and one for output coupling.

2.3 The New Resonator

The newest resonator is the third in a series of designs for a slightly new approach for the split-ring assembly. Many of the features of the 3.7 GHz design are still in place. These include, the Pb:Sn electroplated surface, the shielding tube, inductive coupling in transmission, and the angled form of the top of the resonator used to distance the sample from the large E fields present within the gap. The shielding tube has a diameter of 11/16" for which the lowest mode of propagation occurs at 10.1 GHz. The tube is closed some distance below the rings but is open above them to allow for the insertion of the sample. When one considers the lowest mode of propagation, while operating at frequencies from 910 MHz to 2.4 GHz, the RF fields attenuate with a decay length of $\sim$3 cm. If one considers the TE_{01} mode of propagation, which is the mode most likely to be

driven by the resonator, the decay length decreases to ~1.4 cm. Thus, the RF power, being proportional to the square of the fields, will diminish by a factor of 100 before reaching the unplated copper top plate positioned 1.3" from the end of the rings.

There are, however, significant changes in the design of the new resonator. Most of the differences stem out of the desire to eliminate the previous problem with weak links associated with assembling the RF surface in pieces. Instead of a full ring with one gap, this resonator uses two diametrically opposed gaps formed by two half rings. A sapphire plate is used to size the gap and further lower the frequency. Since the two pieces of the ring are not in electrical contact, the problem of RF currents running across a mechanically pressed joint has been eliminated. With the ring in two pieces, it is easy to electroplate the entire surface of the ring, including the gap face. (Plating of the gap surface would not be possible on a single gap resonator constructed by cutting a narrow gap out of a single piece of copper.) The ring is held in the centre of the shielding tube by two sapphire posts that feed through the walls of the shielding tube and locate into shallow blind holes in the sides of the ring halves. The compression of the sapphire posts is set by screws on the exterior of the shielding tube.

It is particularly advantageous to be able to adjust the position of the sapphire supporting posts. This makes it easy to reassemble the resonator with a different size of sapphire plate in the gap to operate the resonator at a different frequency without having to worry about difficulties in obtaining a tight fit for the entire assembly. In fact, in addition to changing the sapphire plate in the gap, the entire ring assembly can be replaced with one of different dimensions. Since this only entails machining 2 small half rings, operating this resonator at different frequencies is cost effective.

The drawings of the resonator shown here are of the third and final version of prototypes. It was found that the centre portion of the resonator, which includes the cutoff tube and support for the split ring, had to be designed so as not to have any blind holes

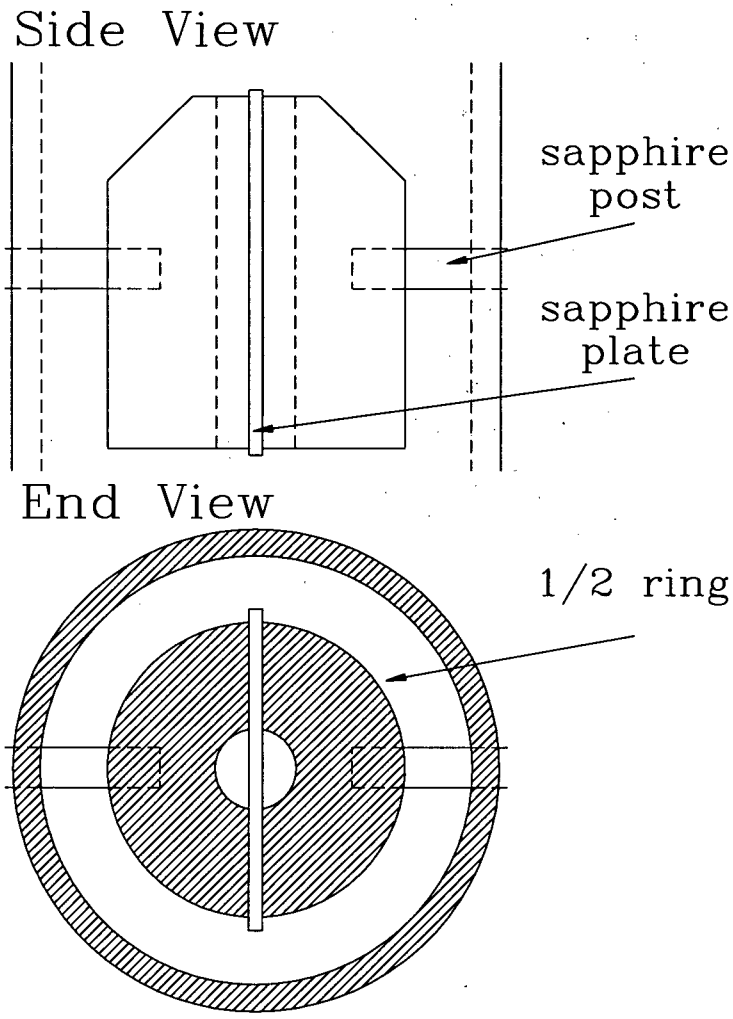

Figure 2.4: The New Resonator - Close up of the rings and plate only

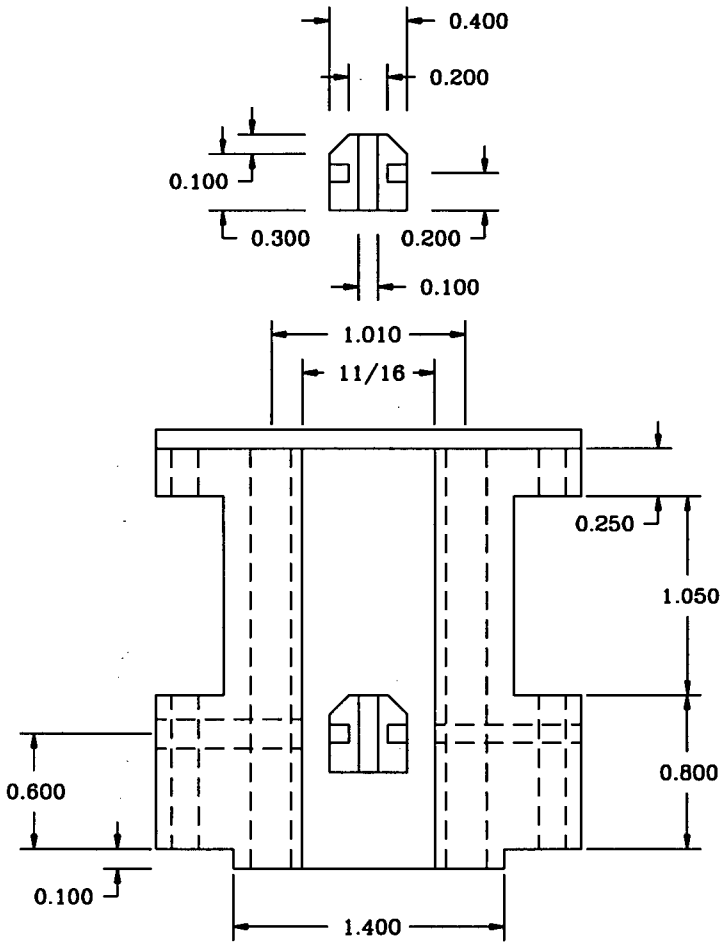

Figure 2.5: The New Resonator - With Sapphire Support Posts

Ring Set	r_O	W (Gap Width)	t (Gap Thickness)	Frequency (GHz)
1	0.050"	0.150"	0.004"	2.4
2	0.075	0.190	0.004	1.4
2	0.075	0.190	0.002	0.91

Table 2.1: Measured Resonant Mode Frequencies for Various Ring Set-Ups

which tended to accumulate acids during the electroplating process and subsequently degrade the surface of the resonator. The length of the resonator core in the third version was increased to move the joint with the bottom cap further away from the resonator. Although the shielding tube is beyond cutoff and the currents on the walls of the tube should be essentially perpendicular to the axis of the ring, having the bottom cap closer to the resonator tended to cause a slight power dependence of the Q factor that was likely due to a minor weak link problem in the outer conductor.

2.3.1 Calculations of Frequencies

With two choices in both ring sets and sapphire gaps, several different frequency options have been tested. The results are given in table 2.1. In order to ensure that the field patterns near the sample are consistent in size from one frequency to the next, it is desirable to maintain a consistent bore size for the rings. In light of this constraint, the 910 MHz arrangement represents a reasonable lower limit on the frequencies available.

The thin sapphire (0.002") and the reduced amount of space between the rings and the shielding tube make this particular arrangement much more tedious to assemble than the higher frequency options.

Higher frequencies than those that have been tested are obtainable by moving to larger gap sizes which are easier to assemble. In fact, by moving to a mostly vacuum 0.004" gap (using small shims to keep the rings in place) with the second ring set that is

already in use, the resonant frequency should be ~4.6 GHz.

On one occasion, when operating with the second ring set with the thinner 0.002" sapphire, one of the gaps was accidentally shorted giving a frequency of 650 MHz which is consistent with increasing the total capacitance by a factor of two which is as expected since the two capacitive gaps are in series.

The actual resonant frequencies of the split-rings differs slightly from the theoretical values for infinite length which is not at all unexpected considering the fact that the length is only roughly equal to the overall width and the top has been machined with a chamfer.

2.3.2 Electroplating the RF Surfaces

The resonator pieces are machined and polished from OFHC copper. Solvents and an ultrasonic bath are used for cleaning before being briefly soaked in a Cu etch solution of 20% HNO_3, 55% H_3PO_4, 25% CH_3COOH. After soaking in NaOH for 30 minutes, the surfaces are again briefly etched, this time with a Lead stripping solution of 20% H_2O_2, 80% CH_3COOH.

After thorough rinsing, the pieces are then immersed in the electroplating solution. This solution contains lead fluroborate $Pb(BF_4)_2$ (diluted to 100 g Pb / litre)) with tin electrochemically dissolved in at the 5% level with respect to the lead content. In the role of a surfactant, a small amount (0.2 g/litre) of mucilage glue is corralled into the mix to reduce the growth of dendrites during the electroplating.

The electroplating is performed with current densities of $30mA/cm^2$. Attempts to plate at levels much above this often result in the growth of unwanted dendrites especially near sharp corners in the resonator pieces. Such growths could potentially lower the unloaded Q of the resonator as currents are induced along the rough irregular surface of the dendrite as it sticks out into the RF fields.

After plating, the pieces are removed and rinsed with water and acetone before being quickly blown dry to avoid water stains. A good session of electroplating results in a surface that is light grey in color and matte in appearance both immediately after the plating and even months later. A plated surface that turns in color to a dark grey color is indicative of a contaminated plating solution.

The plated surfaces can be polished after plating by inserting an acetone soaked Q-tip in a hand held Dremel tool. Although polishing does remove water stains and light scratches in the surface caused by handling, it has not consistently proven to improve the Q factor.

Replating pieces that have already been plated follows the same procedure as above without the use of the etchants. Hand polishing before replating was often done to expose a clean Pb:Sn surface. In addition to helping the surface to accept new material, this also provides a visual clue during plating as to which surfaces have and have not received a coating.

Chapter 3

Results for the Resonator

3.1 First Resonator

Prototypes of the double gap design began with a one piece outer body that was machined out of brass. Compared to copper, electroplating onto brass is more difficult but the relative ease of machining allowed for quicker testing of the double ring with sapphire support. In addition to the extra difficulty in obtaining a good Pb:Sn finish on the brass, the electroplating was hampered by two other design flaws.

Firstly, the use of blind tapped holes in the area where the bottom cap was attached created opportunities for the etchants to become trapped, later degrading the finished surface. Also, the large size of the one piece made the electroplating physically awkward. Most of these difficulties can be attributed to the weight and size of the large 3.75" wide flange (visible on the right in figure 3.6) to which the vacuum can is attached from underneath.

First tests of the resonator did, however, show promise in terms of the physical stability of the ring support design. The resonator showed no signs of microphonics at a level which could affect future measurements with samples. Even abrupt thumps on the dewar did not offset the stability of the resonant frequency. However, the results for the unloaded Q factors, shown in table 3.2, were disappointingly low.

Assembly of the resonator was not difficult as the center of the split-ring was only 0.400" from the end of the shielding tube and the clearance between the edge of the ring

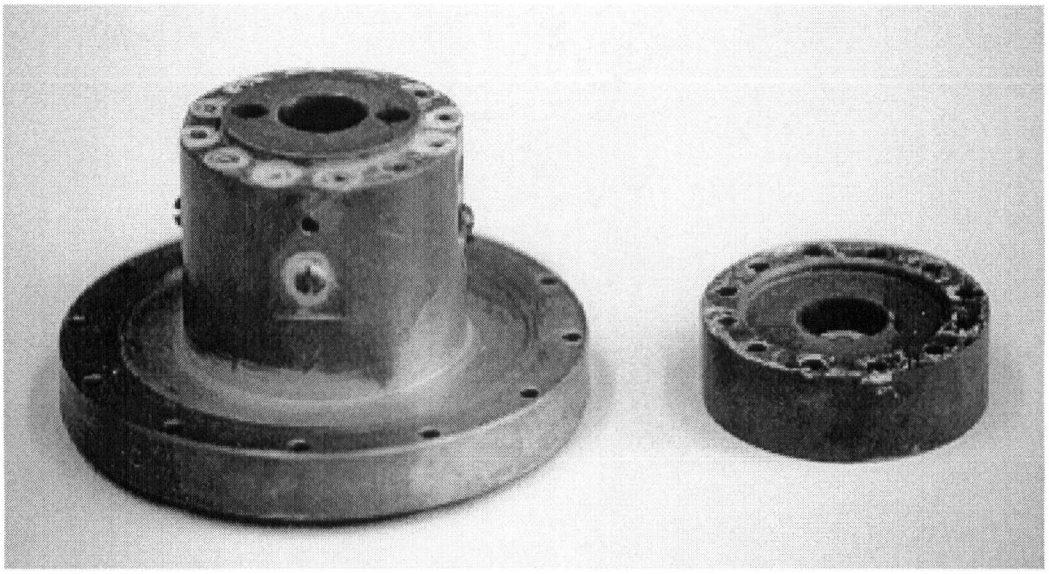

Figure 3.6: Photo of the original design. On the left is the upper portion with the large vacuum flange and on the right is the bottom cap. Corrosion from etchants is clearly visible.

Run No.	Frequency (GHz)	Qo	Comment
1	2.13	237 000	
2	2.10	274 000	replated
3	2.24	703 000	replated and polished

Table 3.2: Results for Q at 1.2 K for the first prototype resonator

and the shielding tube was 0.144". Upon taking the resonator apart, there was some breakage of the sapphire posts that hold the rings in place. The breakage tended to occur on the ends of the posts that were in contact with the set screws. All subsequent assemblies on this and other versions of the resonator used small cylindrical slugs as spacers between the irregularly shaped set screws and the flat edge of the posts. The slugs where machined from copper and plated with the Pb:Sn compound.

Due to the fact that the thermal contraction of the sapphire is less than that of the metal rings and shielding tube, the pressure exerted by the posts to hold the ring together increases when the resonator is cooled to liquid helium temperatures. Essentially, it is this increase in compression that leads to the sturdy nature of the operation at low temperatures. It also causes the face of the gaps on the rings to develop a mechanically polished appearance after the first run following a replating.

3.2 Second Resonator

Attempting to improve on the shortcomings of the first resonator, several key changes were made in the design and fabrication of the second resonator. Addressing the issue of obtaining a good electroplating finish, and therefore a high unloaded Q factor, led to switching to copper for machining and to separating the bulky top plate from the rest of the shielding tube.

By splitting the piece in two, the blind holes on the top of the piece were removed from the plating process as was the weight associated with wide vacuum flange. The blind holes at the bottom portion of the shielding tube, now referred to as the "core", were removed by redesigning the joint with the bottom cap to incorporate a small flange containing only "clear" holes from which it was much easier to rinse etchants. The core of the redesigned resonator is now entirely free of the troublesome blind holes and is much

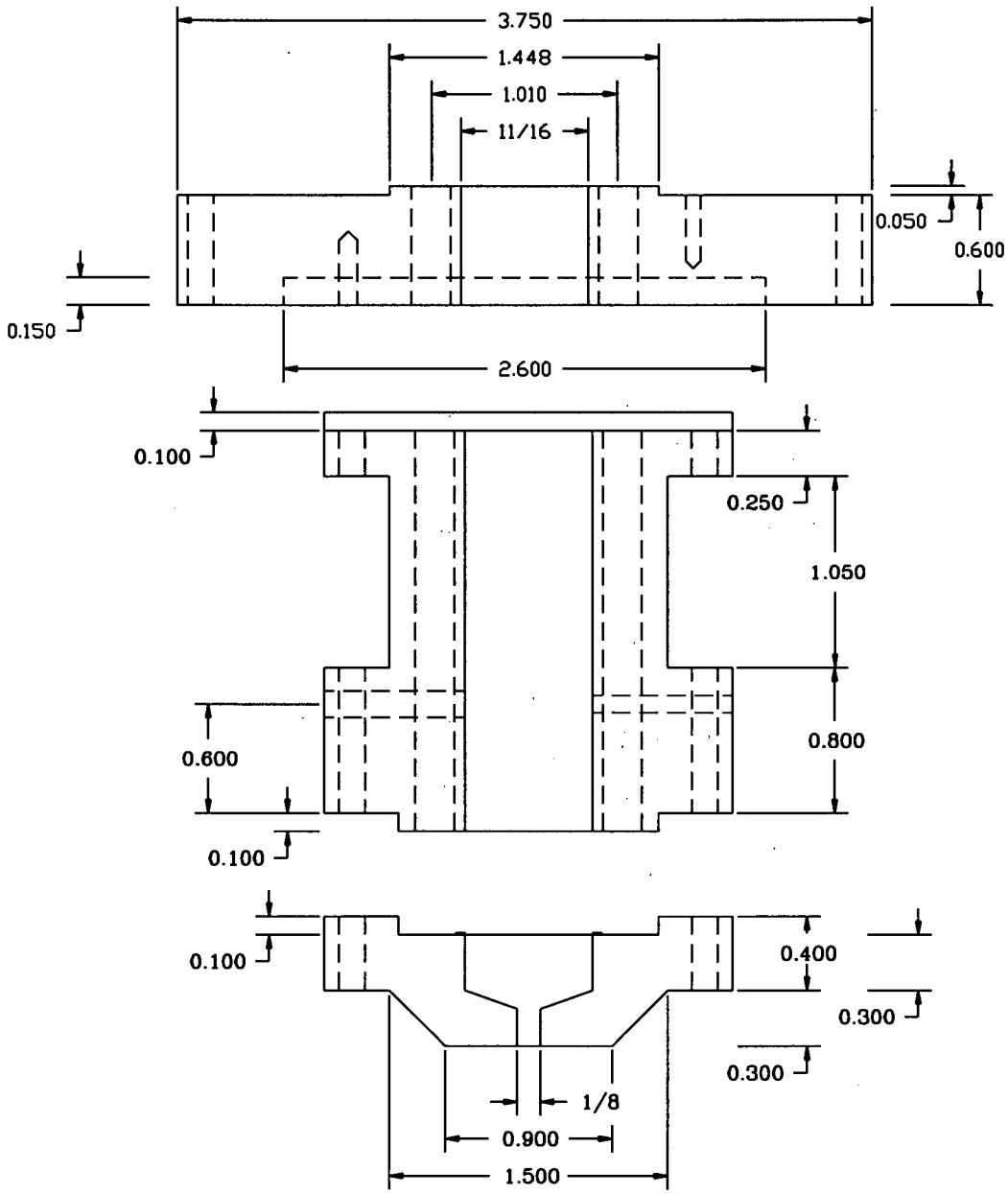

Figure 3.7: Drawing of the 3 pieces stacked together

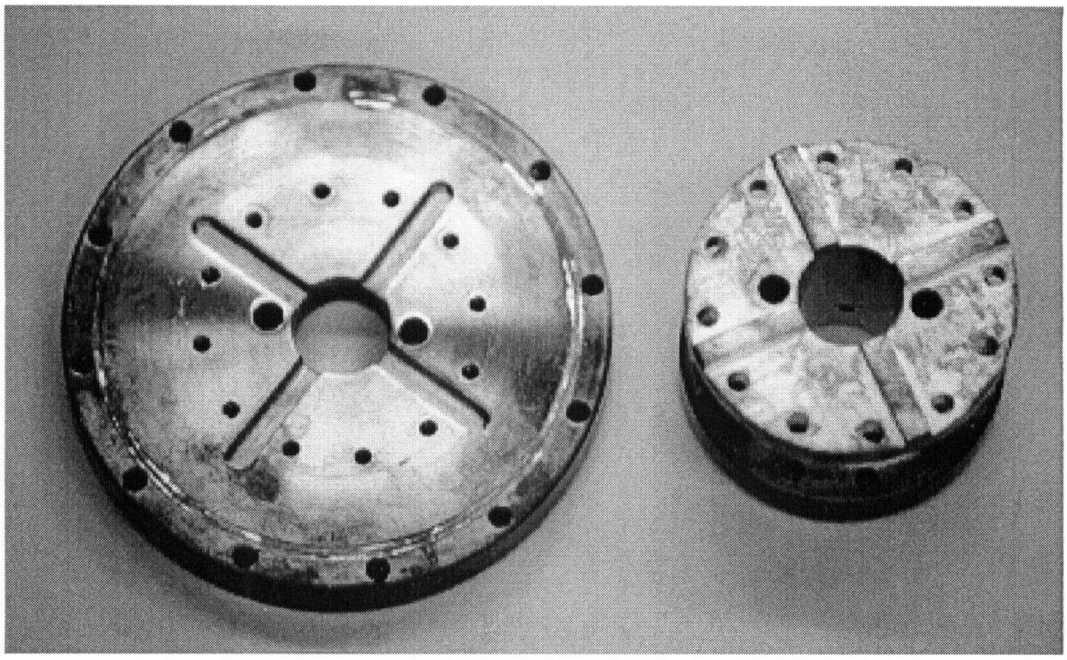

Figure 3.8: Photo of the bottom of the top plate and the top of the core of the resonator. The tongue and groove system aligns the tubes used by the coax.

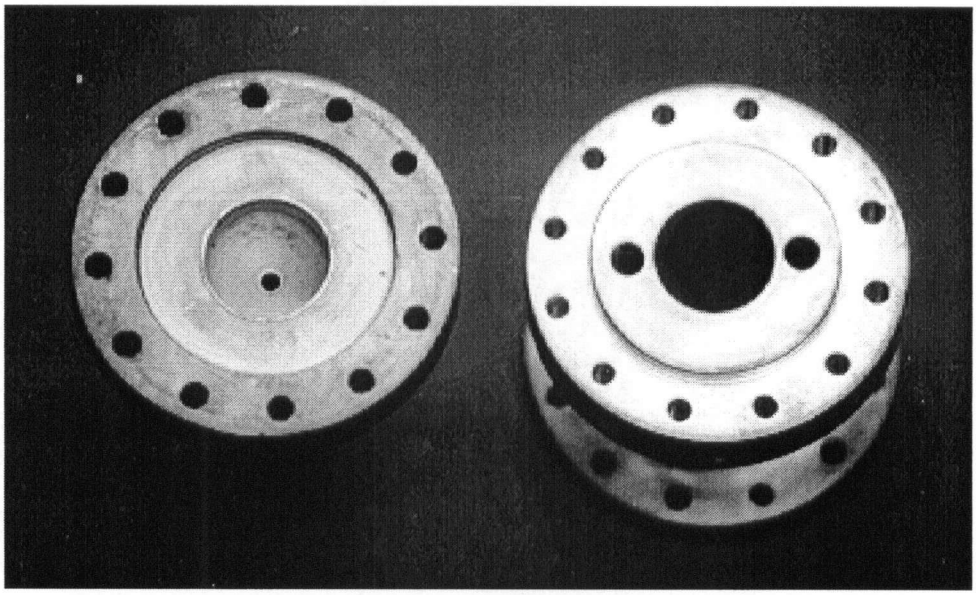

Figure 3.9: Photo of the joint between the core and the bottom cap

lighter and smaller than before which makes it easier to handle during electroplating. The joint between the core and the top plate uses a "tongue and groove" alignment system that has the groove deliberately machined deeper than the tongue to create four additional pumping ports to the vacuum space within the outer vacuum can. This allowed for much greater pumping speeds than what was possible from the small 1/8" hole in the bottom cap of the shielding tube. The hole in the bottom cap is still not without use. In addition to serving as a drain during the blow off stage of the electroplating, it has on more than one occasion provided an exit for small fallen samples thus allowing for several more runs before the resonator needed to be disassembled.

Low temperature testing of the second prototype revealed consistently higher unloaded Q factors than for the previous brass version. Like the first prototype, this resonator was physically robust and showed no sign of microphonics at a level which would affect measurements with samples. Unfortunately, this was not true for the sample holder

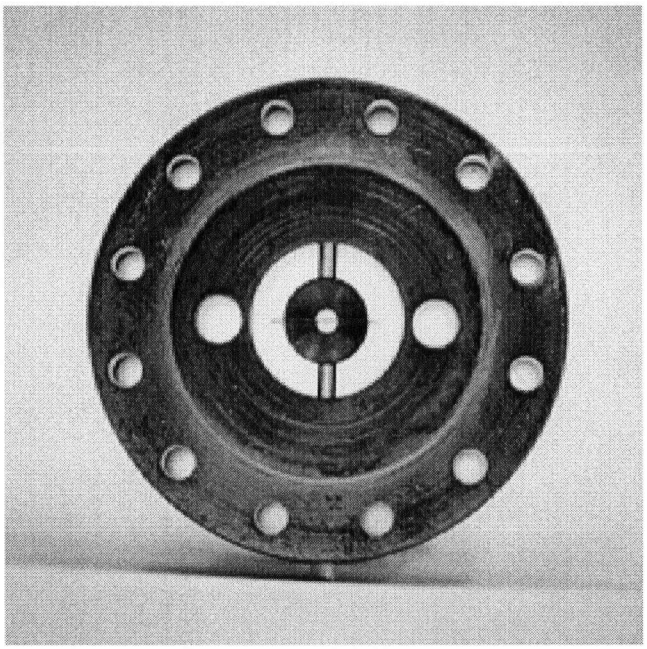

Figure 3.10: Photo of the rings in place within the core also showing the holes used by the coax. The two sapphire support posts are visible above and below the rings. Small coupling holes link the coax hole with the central shielding tube.

Run No.	Frequency (GHz)	Qo	Comment
1	2.42	2 346 000	-
2	2.42	2 563 000	-
3	2.38	805 000	replated
4		3 000 000	replated
5	2.28	2 800 000	-
6	2.28	2 250 000	-
7	2.30	2 420 000	-
8	2.27	2 757 000	-

Table 3.3: Results for Qo at 1.2K for the second prototype resonator

positioned above the resonator during measurements and this was a motivating factor for developing the time-domain method of measurement described in Chapter 4.

Surprisingly, the resonator exhibited a power dependence, shown in figure 3.11, in the unloaded Q factor to a degree that suggested that weak links were present at some location on the RF surface. With no joints in the superconducting Pb:Sn surface at the rings themselves, the joint in the RF surface where the bottom cap attaches became suspect. In a true TE_{011} cavity mode, all RF currents run perpendicular to the cylindrical axis and should not cross such a joint in the resonator. The split-rings, however, are not entirely cylindrically symmetric due to the presence of the gaps and this symmetry breaking could lead to currents that require traversing the joint as they circle the shielding tube.

3.3 Third Resonator

The third and final resonator contained only one design modification from the second prototype. In efforts to reduce the power dependence of the unloaded Q factor, the length of the shielding hole from the location of the rings to the joint with the bottom cap was increased by 0.200". Although this makes the assembly of the rings considerably more difficult, it reduces the magnitude of the electric fields and currents present at the RF joint. As can be seen in figure 3.12, it was now possible to have no detectable power dependence over a 10 dB range in the RF power. Although figures 3.11 and 3.12 do not necessarily represent the same power level within the resonator, it was not possible to find any such working range of power with the previous resonator.

The third resonator, like the second, was also machined out of copper with the exception of the rings for which niobium was used in hopes to exploit the higher T_c of 9.2 K and therefore lower microwave loss at the operating temperature of 1.2 K. Without

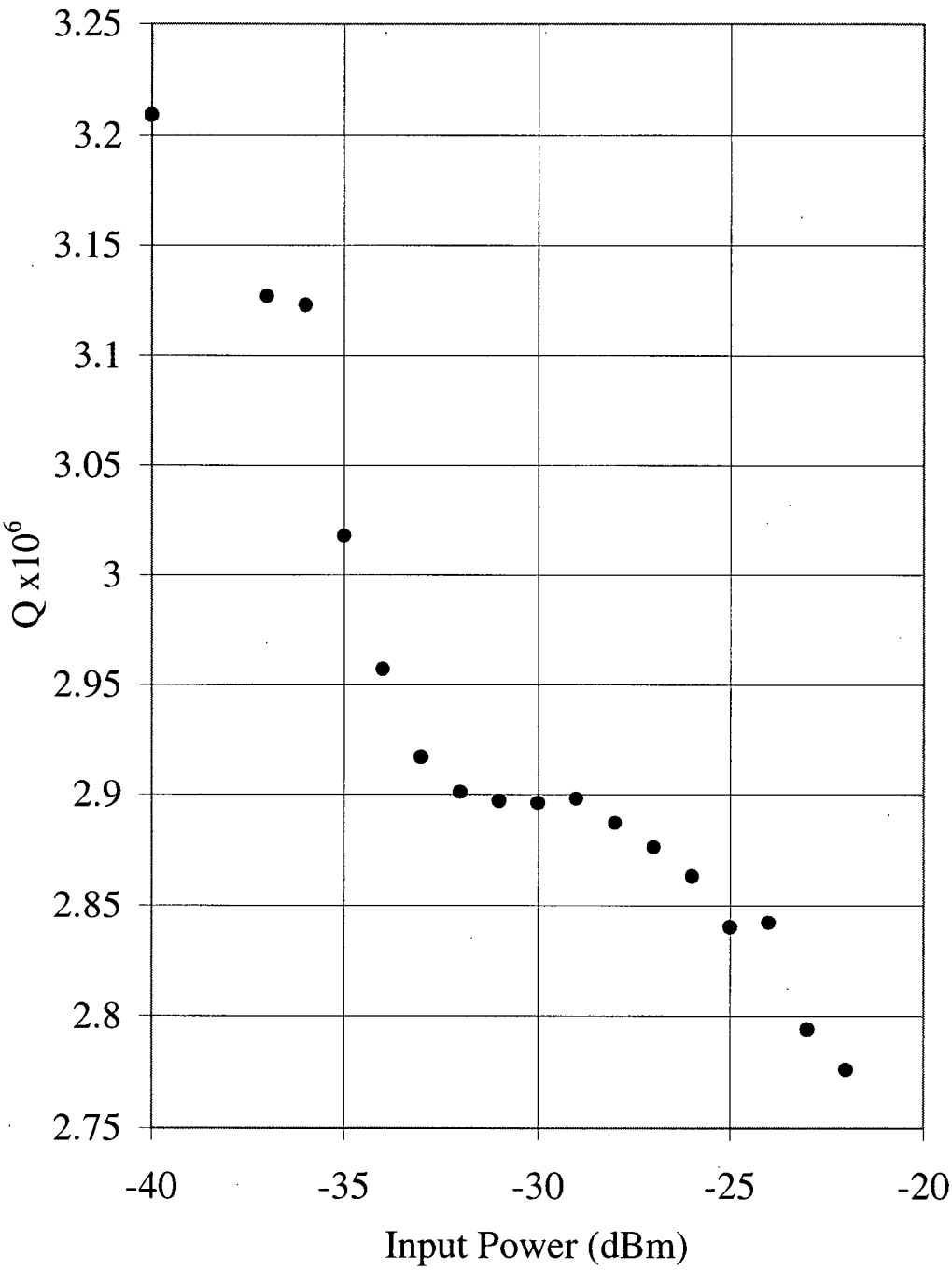

Figure 3.11: Power dependence of the unloaded Q Factor for the second prototype

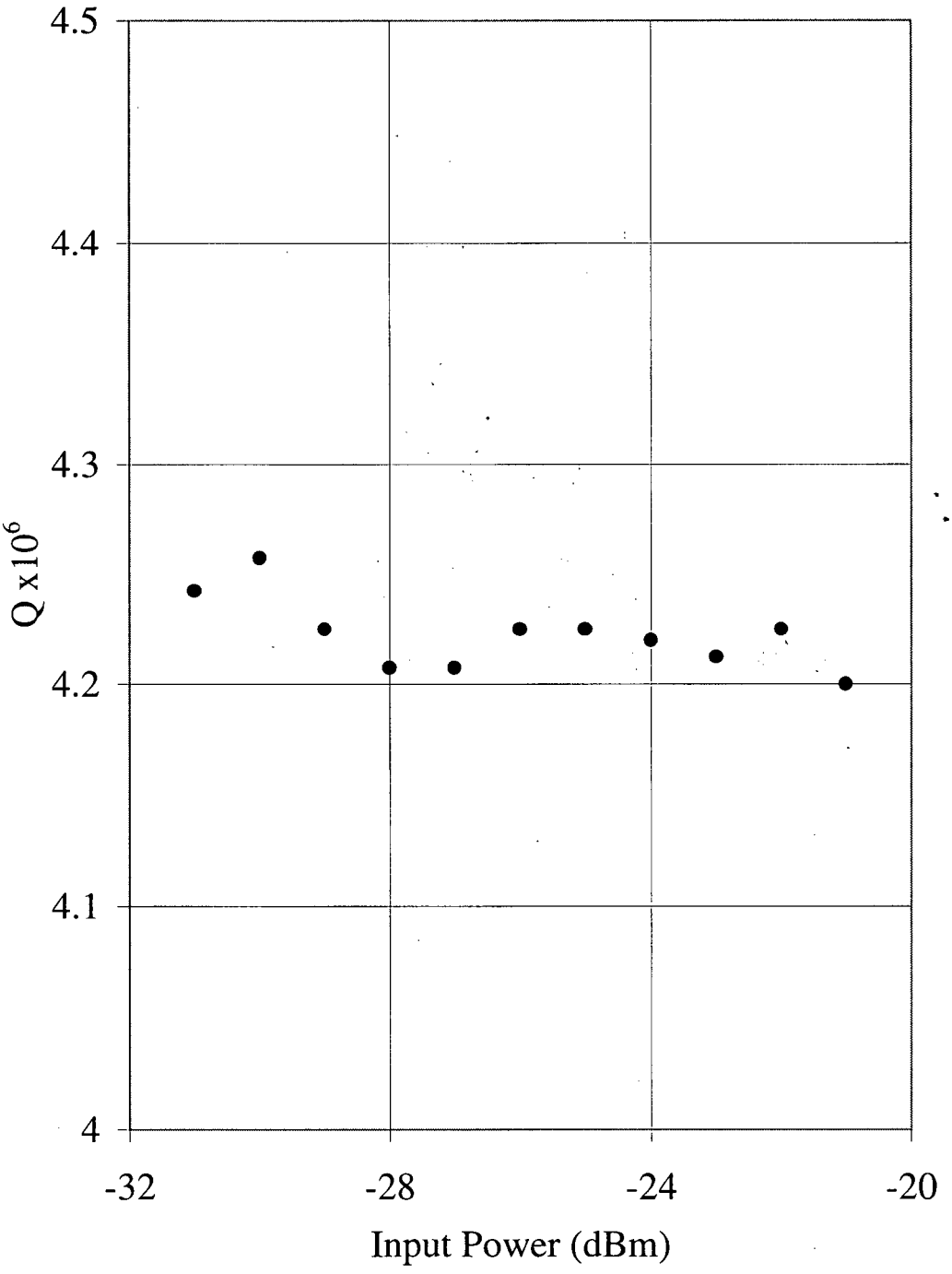

Figure 3.12: Power dependence of the Q factor for the third prototype.

the aggressive cleaning process necessary to prepare a clean niobium surface, the results for the niobium rings were disappointing and remaining tests and measurements of the third resonator were all performed with the Pb:Sn plated copper ring set from the second resonator.

With the rings from the second resonator in place, the Q factors, which always vary slightly from one plating to the next, were consistently high enough to measure the low losses of the four $Tl_2Ba_2CaCu_2O_y$ thin films provided by *Superconductor Technologies* of Santa Barbara, Califonia, USA (STI). Surprisingly, there were several instances where the unloaded Q factor improved from run to run without the RF surface being replated. This increase may be attributed to the plated surface out gassing some lossy component deposited during the electroplating.

Although this resonator is no longer hampered by an unloaded Q factor that is RF power dependent, the Q is dependent on the temperature of the sample even though the sample is not in direct thermal contact with the resonator. The dependence arises out of a slightly increased helium bath temperature as the sample is heated. The heating problem is dealt with during the experimental procedure by both regulating the bath temperature and performing more frequent measurements of the Q factor with the sample in the "out" position as described in Chapter 4.

3.3.1 Second Ring Set

With the frequency of operation for the intended application of the $Tl_2Ba_2CaCu_2O_y$ films being in the range of 950 – 1000 MHz, a second set of rings for the final resonator was constructed. Using equation 2.32 with corrections obtained from the 2.4 GHz ring set, the second ring set was constructed with the dimensions given in figure 3.3.1.

The slightly larger size of the new ring set makes for slightly easier plating but the assembly of the rings within the shielding tube is now considerably more tedious due to

Run No.	Rings	Gap	Frequency (GHz)	Qo	comment
1	niobuim	0.004"	2.15	368 000	niobium rings
2	1	0.004	2.39	6 570 000	replated
3	1	0.004	2.39	5 475 000	-
4	1	0.004	2.39	7 849 000	NP $= -9x10^{-9}$
5	1	0.004	2.39	low	-
6	1	0.004	2.36	2 127 000	replated
7	2	0.002	0.65	300 000	sapphire failure
8	2	0.004	1.42	3 800 000	older rings
9	2	0.004	1.42	4 070 000	not replated
10	2	0.004	1.42	4 100 000	replated
11	2	0.004	1.42	3 750 000	-
12	2	0.004	1.44	4 125 000	1 month since run # 11
13	2	0.004	1.45	3 473 000	1 day since run # 12
14	2	0.004	1.44	4 001 000	1 month since run # 13
15	2	0.002	0.912	1 658 000	not replated
16	2	0.002	0.911	1 839 000	-
17	2	0.002	0.910	1 651 000	-
18	2	0.002	0.910	1 305 000	-
19	2	0.002	0.910	1 332 000	-

Table 3.4: Results for Qo at 1.2 K for the third prototype resonator. The first run shown is with the niobium ring set. The calibration on the 4th run revealed the given nonperturbative correction at a 25 MHz frequency shift.

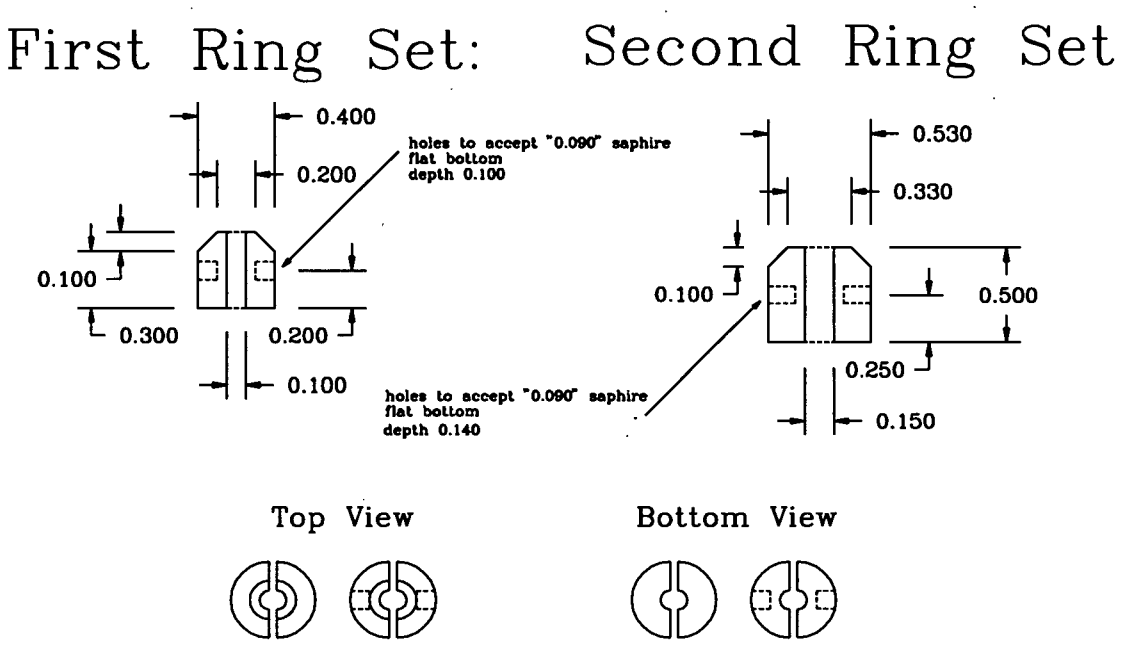

Figure 3.13: Ring Set # 2

the reduced clearance between the rings and the shielding tube which is now down to 0.074". The increased length of the shielding tube of the third resonator adds to the difficulty. Further compounding the troubles is the requirement to use 0.002" sapphire in the gap to create enough capacitance to bring the frequency down to less than 1 GHz.

The thinner sapphire is considerably more difficult to handle than the 0.004" material as it has a much greater tendency to break or slide off of the gap surface. Even with a subtle countersink machined into the blind holes of the rings, attempts to assemble the resonator by inserting the rings and sapphire plate as a whole and then sliding the sapphire posts into place were never as successful as assembling the resonator piecewise. Here success in assembly is measured qualitatively in terms of the number of scratches added to the resonator's surface and fractures to the sapphire plates during the process.

Run No.	Sapphire Thickness	Frequency	Qo	Comment
7	0.002	0.65	300 000	sapphire failure
8	0.004	1.42	3 800 000	older rings
9	0.004	1.42	4 070 000	not replated
10	0.004	1.42	4 100 000	replated
11	0.004	1.42	3 750 000	-
12	0.004	1.44	4 125 000	1 month since run # 11
13	0.004	1.45	3 473 000	1 day since run # 12
14	0.004	1.44	4 001 000	1 month since run # 13
15	0.002	0.912	1 658 000	not replated
16	0.002	0.911	1 839 000	-
17	0.002	0.910	1 651 000	-
18	0.002	0.910	1 305 000	-
19	0.002	0.910	1 332 000	-

Table 3.5: Results for the second ring set

The first low temperature test using the 0.002" sapphire revealed an additional challenge with the thinner material in that it was no longer possible to use one sapphire sheet to cover both gaps between the ring halves. The thinner sapphire is not able to tolerate the compression stresses that develop along the sheet due to the differences in thermal contraction for the copper and sapphire. This stress causes the sheet to fail in the central bore of the resonator where the sheet is not supported. It was just such a failure that caused one of the gaps to become shorted during one of the tests.

As shown in table 3.5, the resonator was also tested and used for measurement while configured with the second ring set and the easier to handle 0.004" sapphire plate offering further evidence that the design offers flexibility in frequency configuration while being robust in terms of microphonics.

Res.	Run	Ring Set	Gap	f (GHz)	ω^2	Qo	Comment
1	3	1	0.004"	2.24	2.7	703 000	replated and polished
2	5	1	0.004	2.28	2.6	2 800 000	-
3	1	niobuim	0.004"	2.15	3.0	368 000	niobium Rings
3	4	1	0.004	2.39	2.4	7 849 000	NP = $-9x10^{-9}$
3	7	2	0.002	0.65	32	300 000	sapphire failure
3	10	2	0.004	1.42	6.8	4 100 000	replated
3	11	2	0.004	1.42	6.8	3 750 000	-
3	12	2	0.004	1.44	6.8	4 125 000	1 month since run # 11
3	13	2	0.004	1.45	6.8	3 473 000	1 day since run # 12
3	14	2	0.004	1.44	6.8	4 001 000	1 month since run # 13
3	15	2	0.002	0.912	6.8	1 658 000	not replated
3	16	2	0.002	0.911	6.8	1 839 000	-

Table 3.6: Summary of results for selected runs for all of the prototype resonators

3.4 Summary of the Results for the New Design

Table 3.6 shows a summary of all of the results for all of the prototype resonators. Included also is the size of the ω^2 factor comparing the frequency of the configuration compared to the existing 3.7 GHz single gap split ring. This value becomes relevant during the frequency dependence analysis in Chapters 5 and 6.

Chapter 4

The Experimental Procedure

4.1 The Perturbation Method

Many aspects of the procedure for measuring the microwave surface resistance have improved from run to run. It is fair to state that the early results are still valid and that the improvements served to both reduce scatter present in the data and to increase the ease with which the results were obtained and not to necessarily improve the accuracy of the measurements. Perhaps the most significant change which preceded all of the final results shown here was the use of time domain measurements of the Q factor of the resonator as described below. Other improvements include measures taken to deal with the tendency of the resonator's Q_O to drift as the sample temperature was increased. The following description of the procedure represents the most recent techniques employed for all of the runs.

The resonator and sample were initially cooled to 4.2 K in the He bath. The bath was pumped to cool the resonator to 1.2K. A second transfer and pumping was prudent as the Q_O was subject to a downward drift if the He bath was not in contact with the mating plate of the resonator. After several hours, the Q_O stabilizes as the sample temperature bottoms out at around 8–10 K.

The resonator is operated in transmission with two inductive coupling loops located in downward passing holes that couple to the resonator by small holes passing from the shielding hole to the coax down holes. The coupling can be adjusted by raising and

lowering the coupling loops within the down hole. Weak coupling is generally preferred as it does not add necessary coupling losses to the resonator thus decreasing the sensitivity of the measurement.

The microwave power is provided by an HP 83620A synthesizer and the transmitted power is measured with a crystal diode detector following a 30 dB microwave amplifier. Working in the "square law" regime of the detector, the resulting signal is proportional to the square of the RF fields and thus the power coming from the resonator.

The perturbation measurement is conducted by measuring the unloaded Q_O and the loaded Q_L of the resonator. As mentioned in Chapter 1, the change in frequency, caused by the presence of the sample, is used to reproduce the position of the sample near the rings for each perturbation. The sample holder, shown in figure 4.16, contains the heater and thermometry for the sample and uses a 1/8" sapphire post to support the sample which is held in place on the end with a small amount of vacuum grease. The sample holder makes thermal contact via brass springs to the shielding tube which at this point is well above the body of the resonator in a thin walled stainless steel tube in contact with the helium bath. The end of the brass springs is just visible on the right side in figure 4.16.

The $\Delta(f)/f$ typically used for the measurements was 1/100, which is larger than those typically used in other perturbation measurements [10] [11] where the value is usually kept to 10^{-3} and 10^{-4} respectively. However, it can be seen in figure 4.17 that the perturbation $\Delta(1/Q)$ as a function of $\Delta(f)$ is consistent in shape over the range of $\Delta(f)$'s used for all frequency configurations. Since the perturbation is not perfectly linear, calibrations are performed at every frequency shift in each measurement.

With the sample in place, pertubation measurements are then performed at each desired temperature. The temperature is controlled with the Lakeshore LTC-20 temperature controller. As the sample temperature increases above 50 K, the associated heating

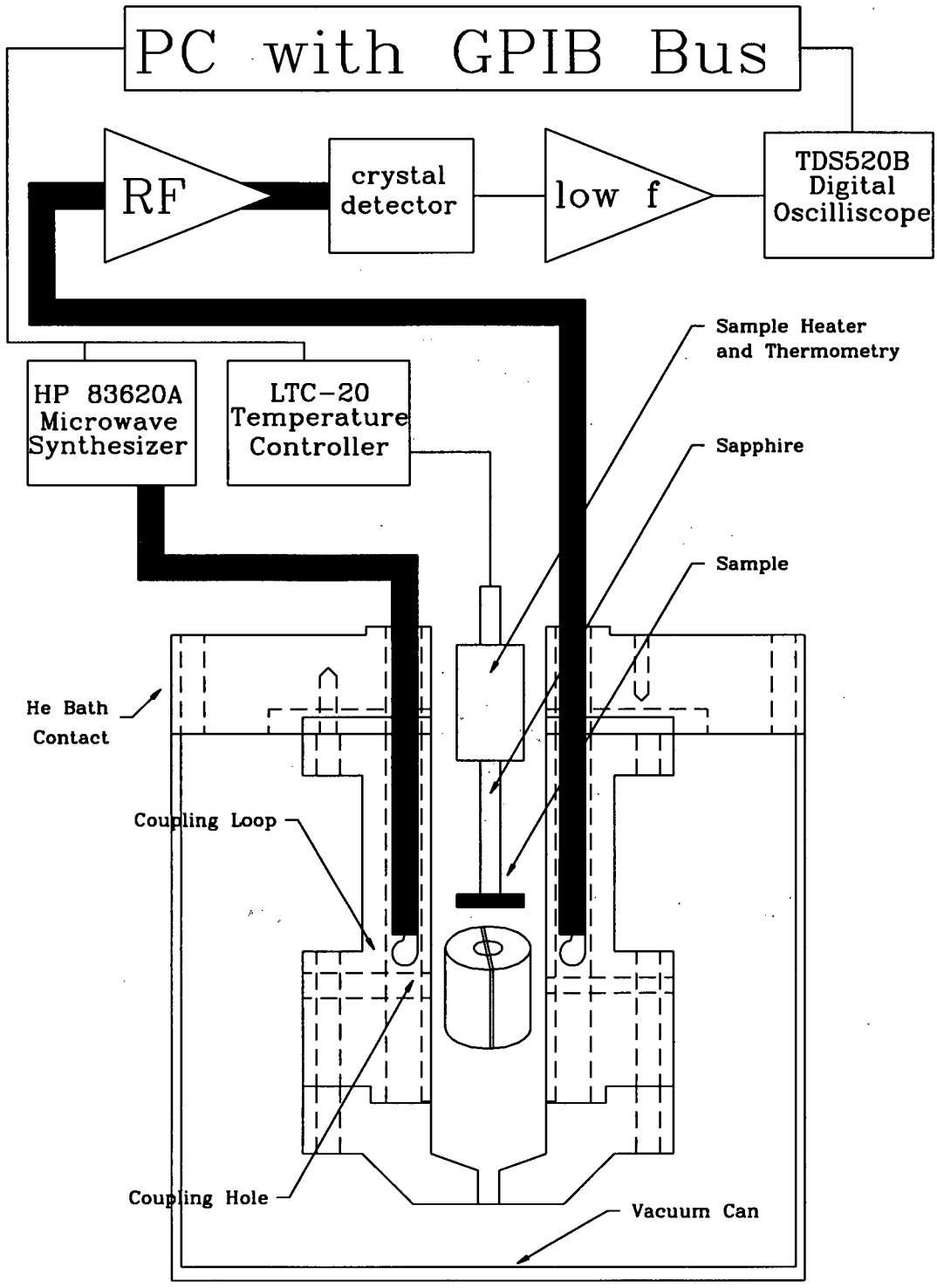

Figure 4.14: Microwave Set-Up

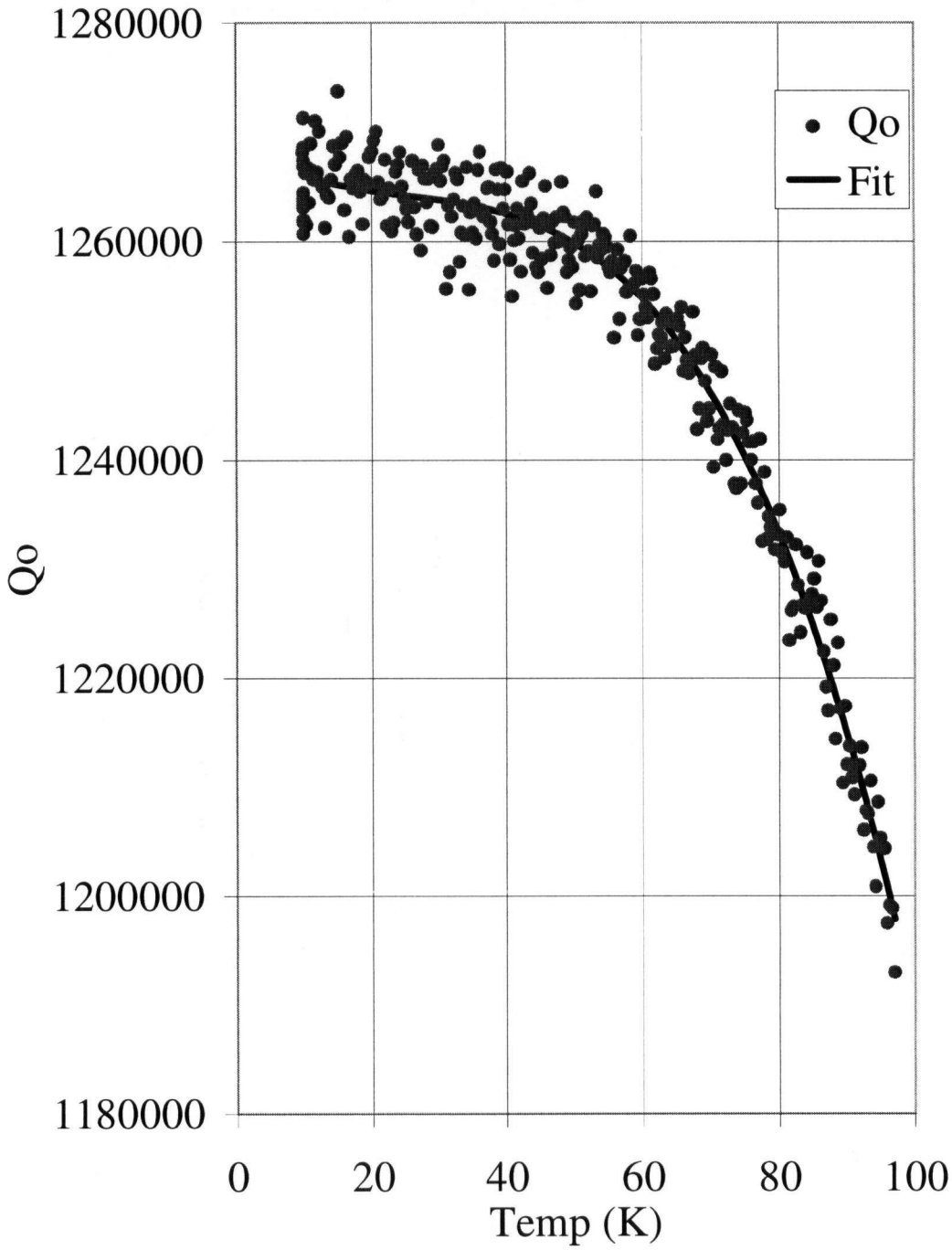

Figure 4.15: Temperature dependence of Qo at 910 MHz including the fitted values

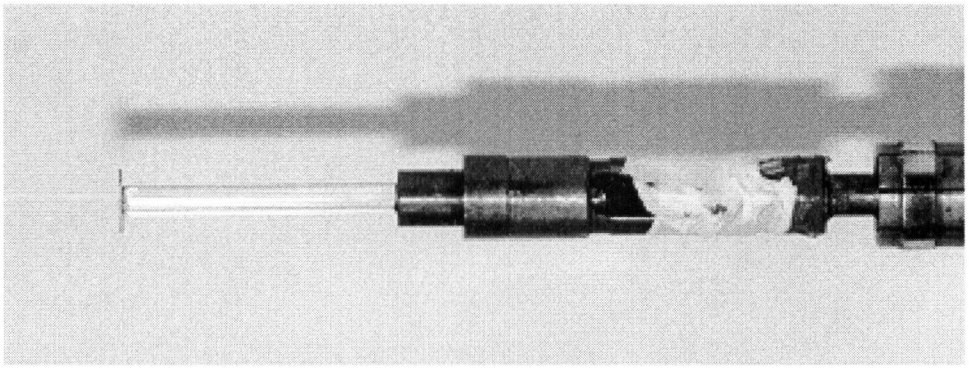

Figure 4.16: Photo of the sample holder used to position the samples near the resonator. The sample holder is also used to regulate the temperature of the sample.

of the helium bath results in a degradation of the unloaded Q factor. Since the degradation is a function of the sample temperature, the Q_O is measured while the temperature is ramped at the conclusion of the run. The data is then fit to a cubic polynomial, as shown in figure 4.15, to obtain values for Q_O as a function of temperature. For $T > T_C$, the sample's losses are so great that small changes in Q_O do not affect the resulting measurements of the surface resistance.

4.2 The Need for Time Domain Measurements

In order to obtain a measurable change in the Q factor when measuring a low loss sample, the sample must be closer to the resonator during the perturbation than is necessary for a higher loss sample. Under these conditions, even small vibrations in the movable sample holder caused by room noises or vibrations from the pumping equipment are enough to play havoc with frequency domain measurements of the Q factor. Such problems with microphonics are not present for high loss samples as they do not need to be inserted as far into the resonator to produce a measurable increase in loss. At these more distant

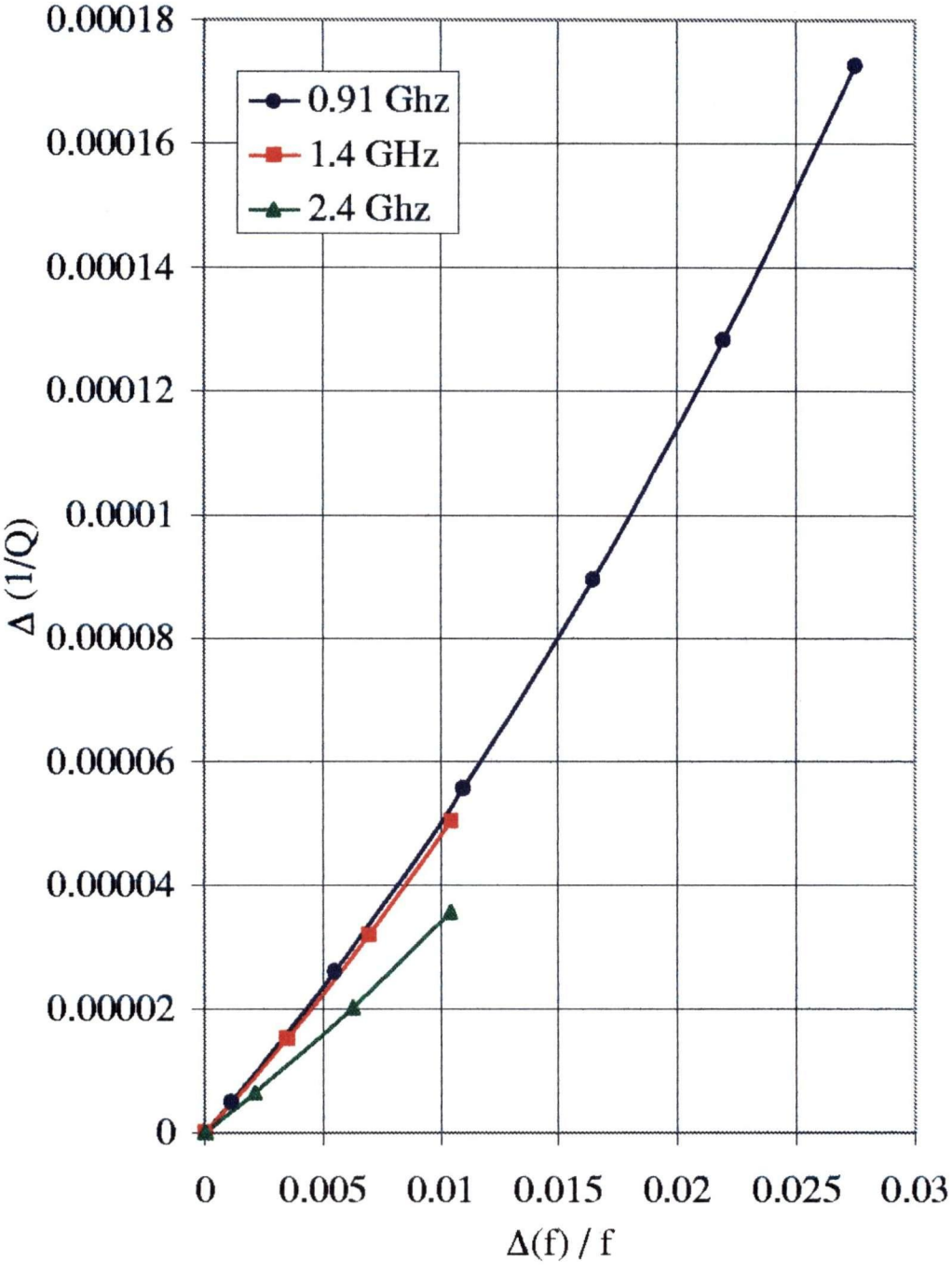

Figure 4.17: Increased losses $\Delta(1/Q)$ as a function of the frequency change in the resonator. All data is on similar sized samples at 20 K.

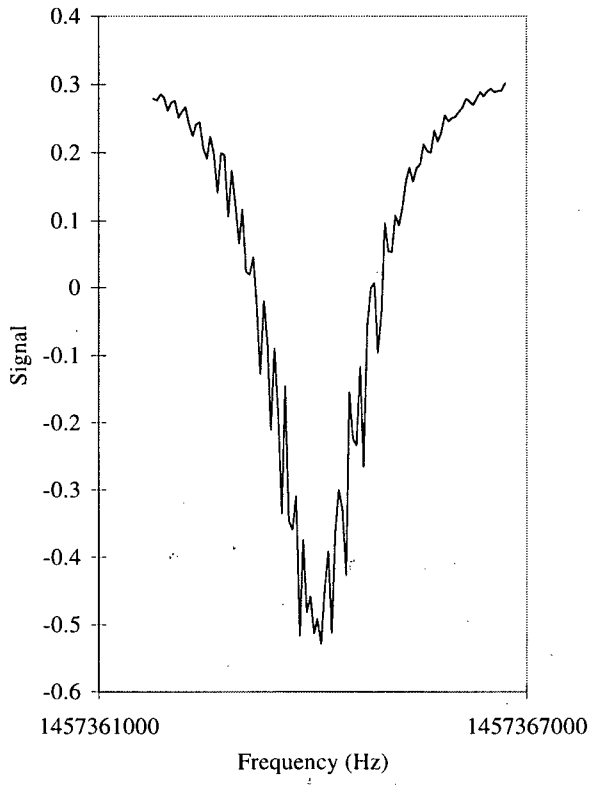

Figure 4.18: A distorted frequency domain wave form due to microphonics in the sample holder.

sample locations, the change in frequency with respect to the change in sample position is much less even though the $\Delta(f)/\Delta(1/Q)$ is essentially constant. Also, loaded Q factors for high loss samples are much lower making them less sensitive to small changes in the resonant frequency.

When viewed in the frequency domain, the expected lorentzian profile is distorted as the moving sample actively changes the resonant frequency during the measurement. As the frequency is swept and the amplitude of the transmitted signal is recorded, the result is similar to the waveform shown in figure 4.18.

With the changes in frequency that are of the order of the resonance bandwidth, it is impossible to obtain reasonable fits to the data that are sensitive to 10–20% changes in the Q factor.

Fortunately, the changes in frequency, although large compared to the width of the waveform, are small compared to the overall $\Delta(f)$. The changes in actual loss due to the microphonics are then small compared to the overall losses in the resonator due to the addition of the sample. With the losses relatively constant, the situation is ideal for measurements of the Q in time domain.

In the time domain method, the resonator is briefly "pinged" with a pulse of RF and then the power within the resonator as a function of time is measured while the resonator rings down. The measurement is still performed in transmission but with the signal now recorded by a Tektronics TDS520B digital oscilloscope. The power curve is then fit to a 3 parameter exponential decay with a DC offset using a non-linear Levenberg-Marquardt algorithm. The DC offset originates with the low frequency amplifier circuit, plus RF amplifier noise rectified by the detector. As can be seen from the close fit to the data in figure 4.19, the microphonics that plague frequency domain measurements do not significantly affect measurements when operating in the time domain.

As described in Chapter 1, relations of importance here are

$$\frac{dE}{dt} = \frac{-2\pi f E}{Q} \tag{4.34}$$

and

$$Q = 2\pi f \tau \tag{4.35}$$

where E is the power stored within the resonator.

The resonant frequency necessary in equation 4.34 is obtained by tuning the RF signal from the synthesizer to obtain maximum power from the resonator after the RF pulse

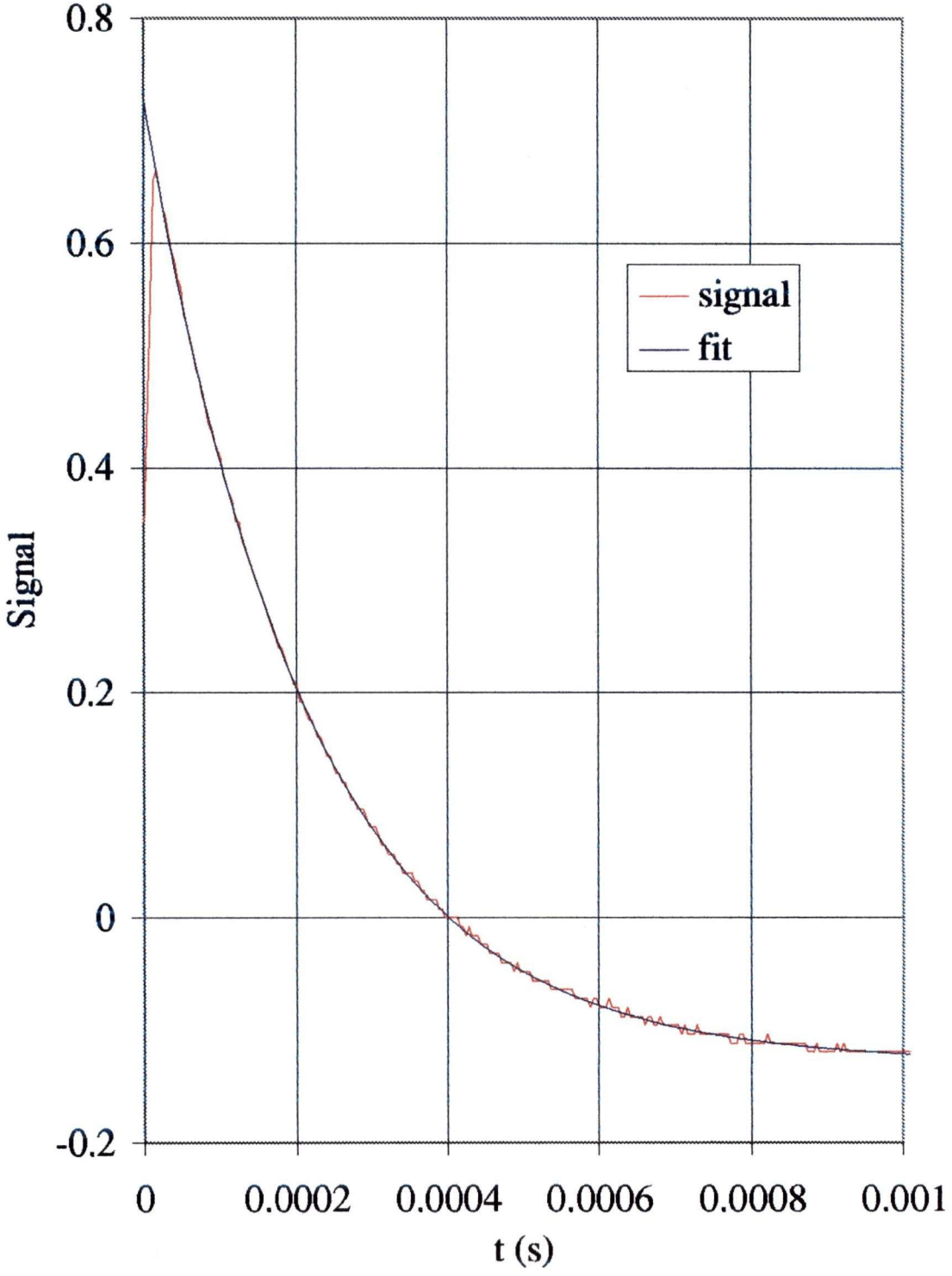

Figure 4.19: Fit to a Time Domain Power Decay Curve

or by briefly switching to frequency domain measurements. Loaded Q factors were then obtained using equation 4.35.

The actual choice of the width of the RF pulse is crucial to the measurement. At first glance it may seem that increasing the length of the pulse would increase the resulting signal from the resonator but this is not necessarily the case if the synthesizer is slightly out of tune with the resonant frequency - something that microphonics ensure. Admittedly, if the pulse is too short, there is not enough time to pump the RF energy into the resonator. If the pulse length is too long, however, its Sinc shaped spectrum in the frequency domain narrows, making hitting the actual resonant frequency of the split ring problematic. Typically, a reasonable balance was obtained at 50 μs where the width of the frequency spectrum of the RF pulse was of order of 10 KHz which is approximately ten times wider than the resonance bandwidth and much wider than the microphonic driven frequency fluctuations.

4.3 Calibration

Calibration of the losses is achieved by performing the measurement on a similar shape and size sample of Pb:Sn. The Pb:Sn sample offers two pieces of information: the absolute loss represented by a given $\Delta(1/Q)$, and the size of the Non-Perturbative correction necessary to correct for the systematic error caused by changing the field pattern with the resonator.

4.3.1 Absolute Loss

The losses of the Pb:Sn sample are measured with the sample in the normal state at temperatures of 20, 50 and 75 K. Although the microwave losses of pure lead can be calculated for any frequency of interest using knowledge of the DC resistivity values at

each temperature, the addition of the Tin at the 5% level requires at least two temperatures to determine the effect of this impurity. The resistivity of the Pb:Sn compound is assumed to be:

$$\rho_{Pb:Sn}(T) = \rho_{Pb}(T) + \rho_{impurity} \tag{4.36}$$

The Microwave losses in the normal state are described by:

$$R_s(T) = \frac{2\pi}{1000}\sqrt{\rho_{Pb:Sn(\mu\Omega)}(T) f(GHz)} \tag{4.37}$$

Experimentally, the microwave surface resistance is given by:

$$R_S = \beta(f)(\frac{\Delta(1/Q)}{\Delta(f)}) \tag{4.38}$$

where $\beta(f)$ is empirically found to be only slightly frequency dependent. Using the ratio of the recorded losses at 20 and 75 K, the value of $\rho_{impurity}$ is determined. The recorded losses at 50 K are used as a check of the validity of the assumption that $\rho_{impurity}$ is temperature independent.

The calibration of the absolute loss was then performed at each of the Δf's used during the measurement. From each separate reference point, a value of $\beta(f)$ was determined and then linearity was used to deal with small changes in $\Delta(f)$ as the sample moves slightly due to thermal expansion and contraction of the sample holder.

4.3.2 Non-Perturbative Corrections

The Non-Perturbative correction is an attempt to deal with the systematic error in the measurement caused by the RF fields and currents repositioning during the perturbation due to the addition of the sample. In addition to screening the sample substrate and sapphire sample holder, the superconducting film also screens the upper portion of the

Frequency Shift	Non-Perturbative Correction
0	0
5	0
15	0
25	$-9x10^{-9}$

Table 4.7: Sizes of the Non-Perturbative correction for the 2.4 GHz configuration.

shielding hole when the sample is in its closest position to the resonator. This might tend to give a loaded Q_L value that is artificially high by the amount equal to the screened loss from the shielding hole.

By backfilling the cavity with a small amount of helium gas, the sample temperature can be lowered to a temperature equal to that of the resonator, near 1.2 K. The Pb:Sn sample at this temperature is lower in loss in comparison to that of the $Tl_2Ba_2CaCu_2O_y$ sample. As a result, when the sample is lowered into measuring position, the Q of the resonator may actually rise. This is due to the fact that the sample screens the sheilding hole thus eliminating losses that are greater than the new losses caused by the induced currents at the sample. The size of $\Delta(1/Q)$ is then recorded at each $\Delta(f)$ position where measurements are taken and used to correct the results for the thin film samples. Figure 4.20 shows the resulting $\Delta(1/Q)$ versus frequency shift for each frequency configuration and table 4.7 shows the resulting (1/Q) correction values obtained for one of the calibrations of the 2.4 GHz configuration of the resonator. The unloaded Q_O was 7.84×10^6 which represents a (1/Q) value of 1.3×10^{-7}.

The method of correction is slightly flawed in the sense that a Pb:Sn sample is used to determine the losses in a Pb:Sn surface elsewhere in the resonator. Ideally this correction would be performed with a "zero loss" sample but the Pb:Sn sample does, nevertheless, provide the upper bound for the nonperturbative correction. In fact, for the two lowest

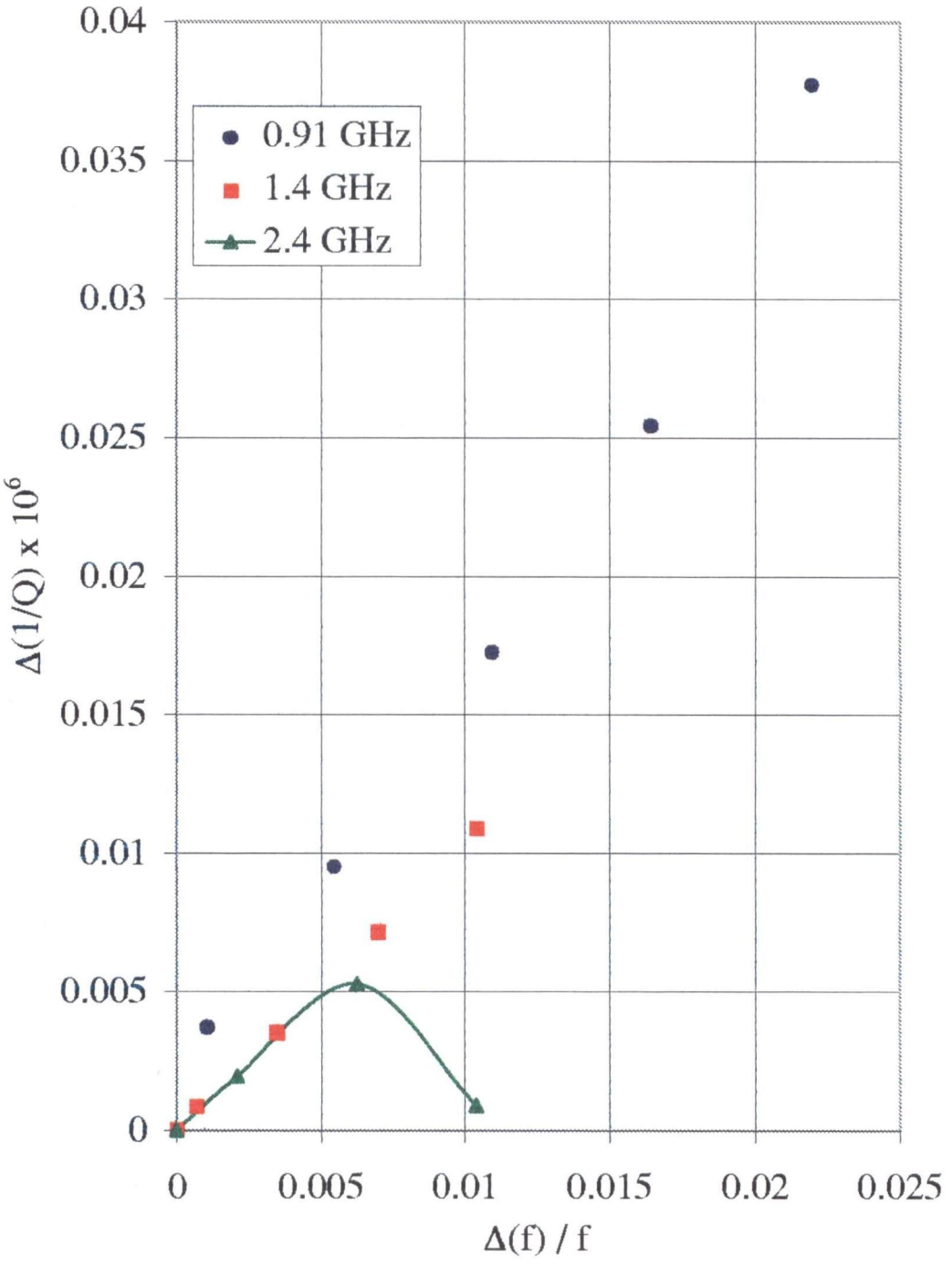

Figure 4.20: Attempt to measure the Non-Perturbative Effect

frequency configurations of the resonator, the measurement of the non-perturbative correction yields straight lines similar to those obtained during calibration thus suggesting that one is measuring actual losses in the Pb:Sn reference sample. These losses correspond to a R_s of approximately 2 micro-ohms which is roughly consistent with the values of 0.5 - 1.8 micro-ohms measured by Dietl[12]. The 2.4 GHz configuration, however, first demonstrates a measurement of real loss at lower shifts, and then a correction due to the non-perturbative effect. Worthy of note is the fact that the size of the correction is only 1/5 of the lowest value measured for the films at that frequency. It is not surprising that the non-perturbative effect shows up the most in the highest frequency configuration as it is here where the decaying RF fields extend furthest up the shielding hole.

Chapter 5

Results for the Thin Films

The four thin film $Tl_2Ba_2CaCu_2O_y$ samples provided by STI were all 4mm circles patterned onto square MgO substrates. The superconducting films were approximately 7000 Å thick while the underlying substrates were 0.38 mm thick. All four samples were cut from the same MgO wafer. Films were deposited on both sides of the original wafer with two sample films from one side referred to as "Up" and two samples from the other side referred to as "Down". The T_c for the films was measured to be 100 ± 0.5 K as measured by AC susceptibility measurements. All results shown here were performed "face up" with the film side closest to the split-ring resonator.

5.1 Microwave Surface Resistance Results

The low microwave loss exhibited by these samples offered many challenges during the measurements. All of the films demonstrated losses in the order of several micro-ohms per square at the lowest frequencies and temperatures.

5.1.1 Results at 910 MHz

The lowest frequency measurements at 910 MHz represented the largest challenge in observing losses in the samples at low temperature. Unlike data from 2.4 and 3.7 GHz, the loss becomes temperature independent not far below the intended operating temperature of 77 K. In fact, below 35–40 K, all four samples demonstrated an upturn in the loss at lower temperatures. The absolute values for the measurement on the Down#3 sample is

somewhat in question due to a lower unloaded quality factor of the split-ring during the measurement. There are also questions about the accuracy of the higher temperatures for the Down#4 and Up #2 samples. The 910 MHz runs were performed with the second ring set and the thinner 0.002" sapphire.

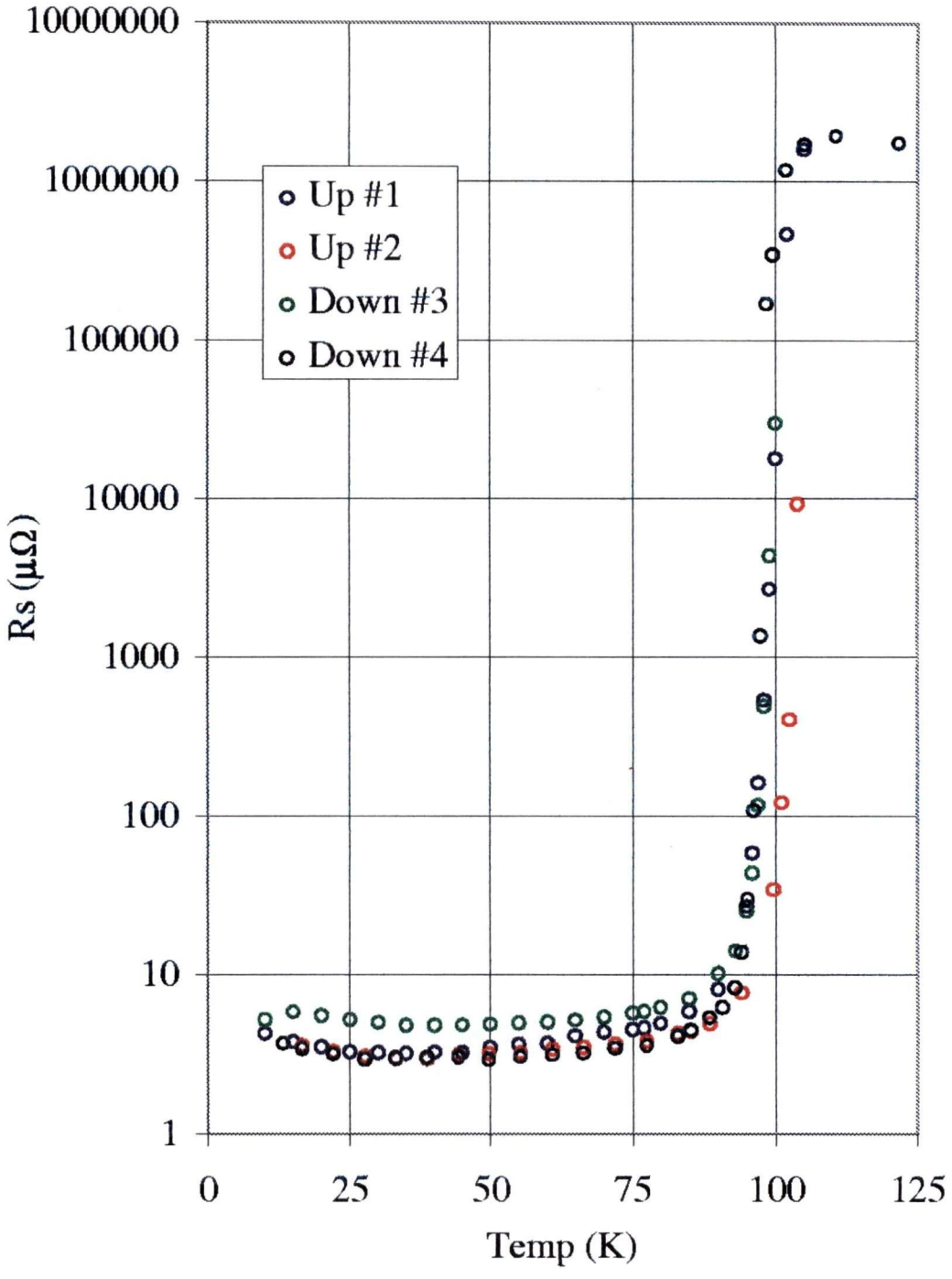

Figure 5.21: R_S for all samples at 0.95 GHZ – SemiLog Plot. The losses for Down #3 and the higher temperatures for Down #4 and Up #2 are somewhat in question.

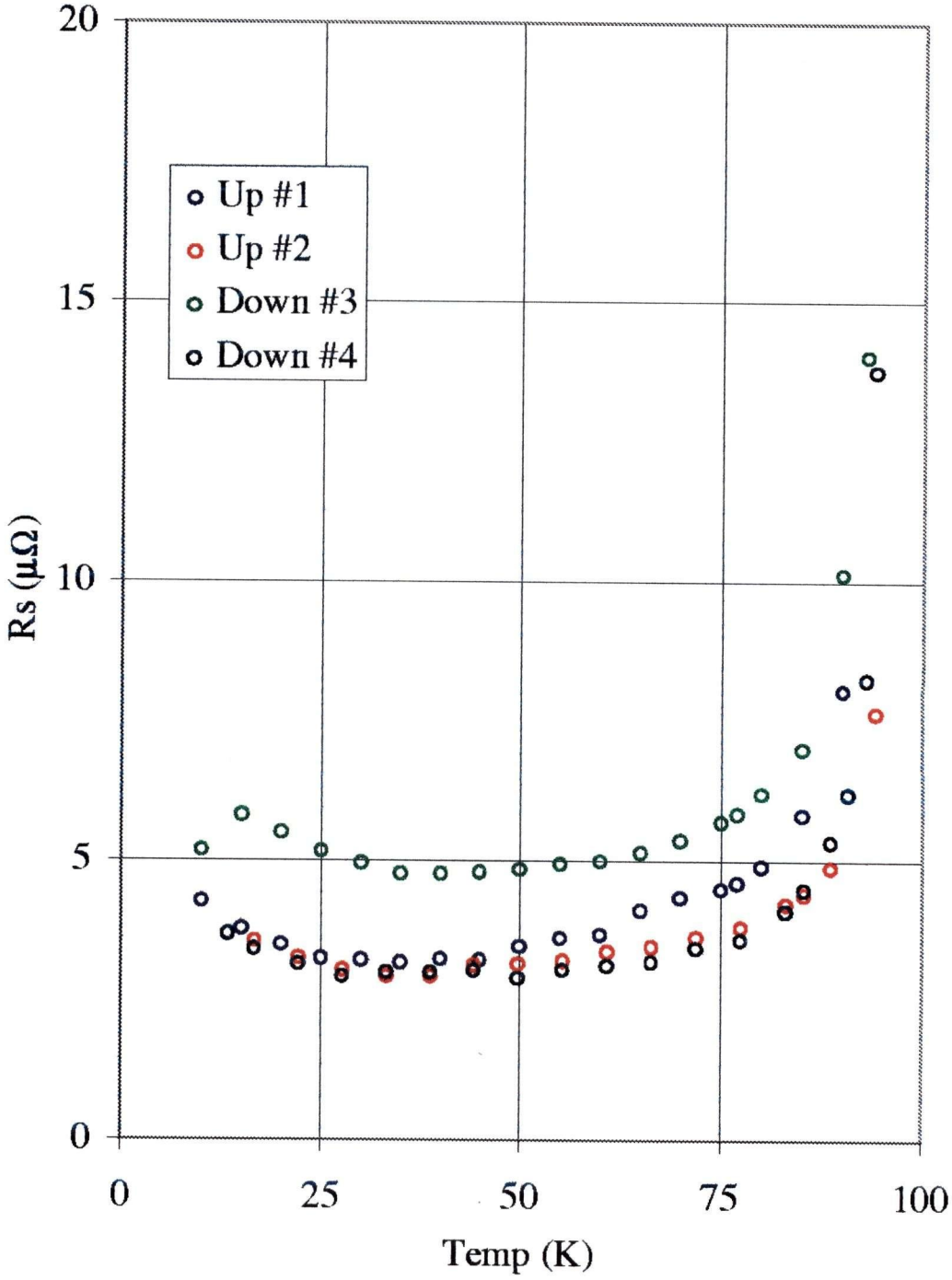

Figure 5.22: R_S for all samples at 0.95 GHZ – Linear Plot. The losses for Down #3 and the higher temperatures for Down #4 and Up #2 are somewhat in question.

5.1.2 Results at 1.4 MHz

The 1.4 GHz runs were performed with the second ring set and the thicker 0.004" sapphire spacer. The absolute value of the losses for the measurement on the Up #1 sample is somewhat in question due to a lower unloaded quality factor compared to the other three measurements. The values for the temperature for the Down #4 sample are also in question at the higher temperatures.

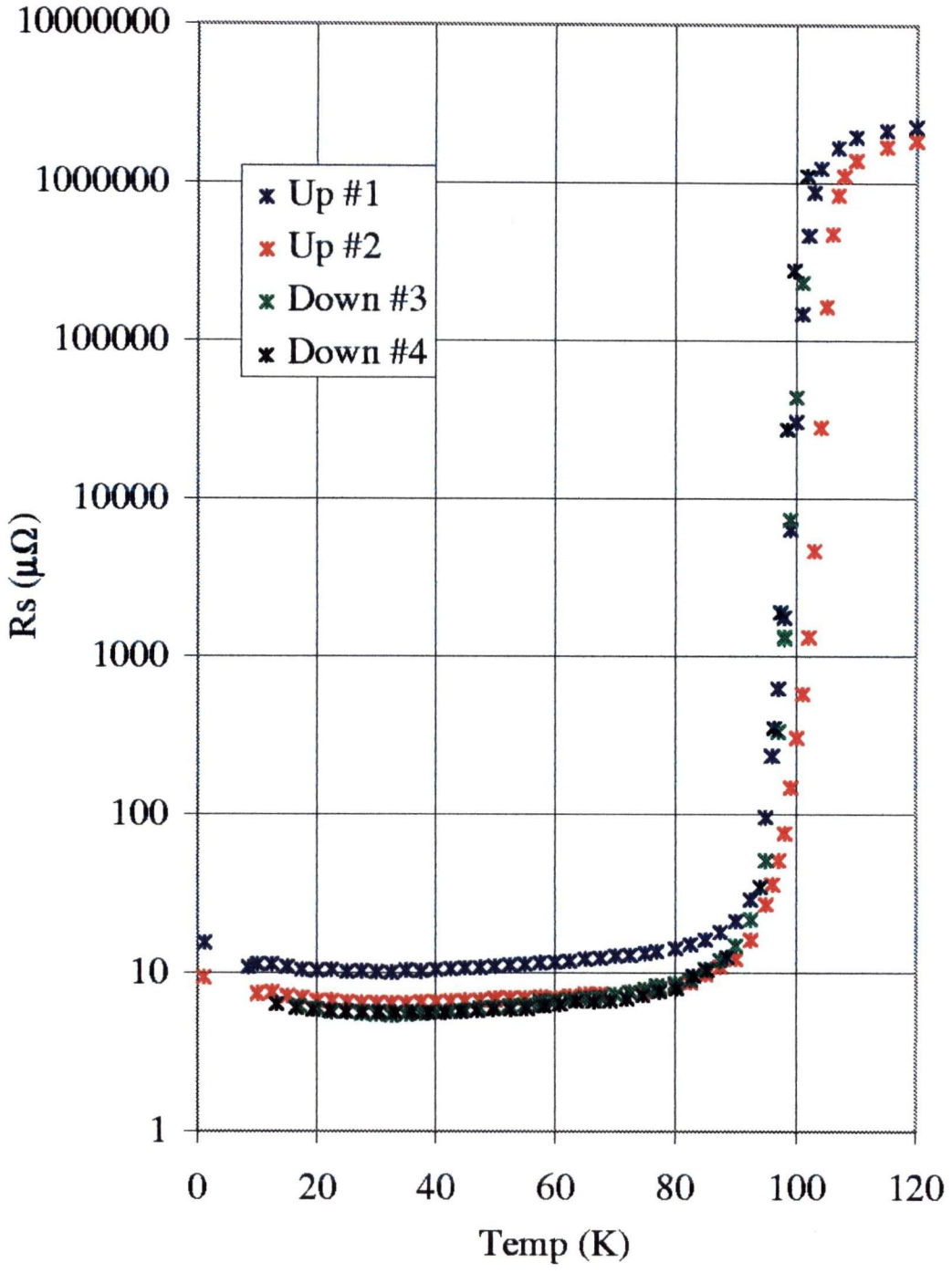

Figure 5.23: R_S for all samples at 1.4 MHz – Semi-Log Plot. The losses for Up#1 and the temperatures for Down #4 are somewhat in question.

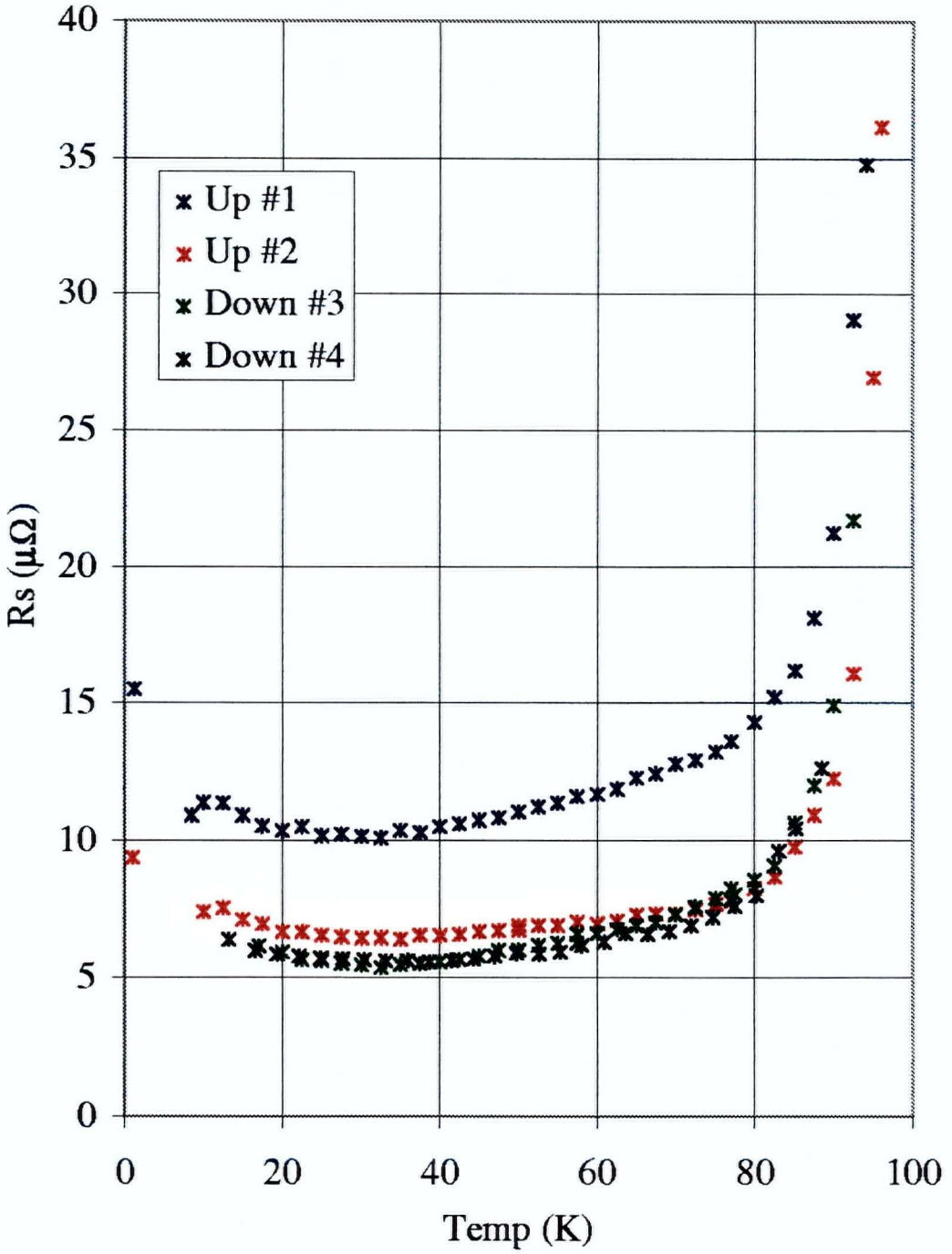

Figure 5.24: R_S for all samples at 1.4 MHz – Linear Plot. The losses for Up#1 and the temperatures for Down #4 are somewhat in question.

5.1.3 Results at 2.4 MHz

The 2.4 GHz runs were performed with the original ring set and the thicker 0.004" sapphire. It is this frequency configuration that has the highest unloaded Q factor of 7.89×10^6 and a resolution of $1\mu\Omega$.

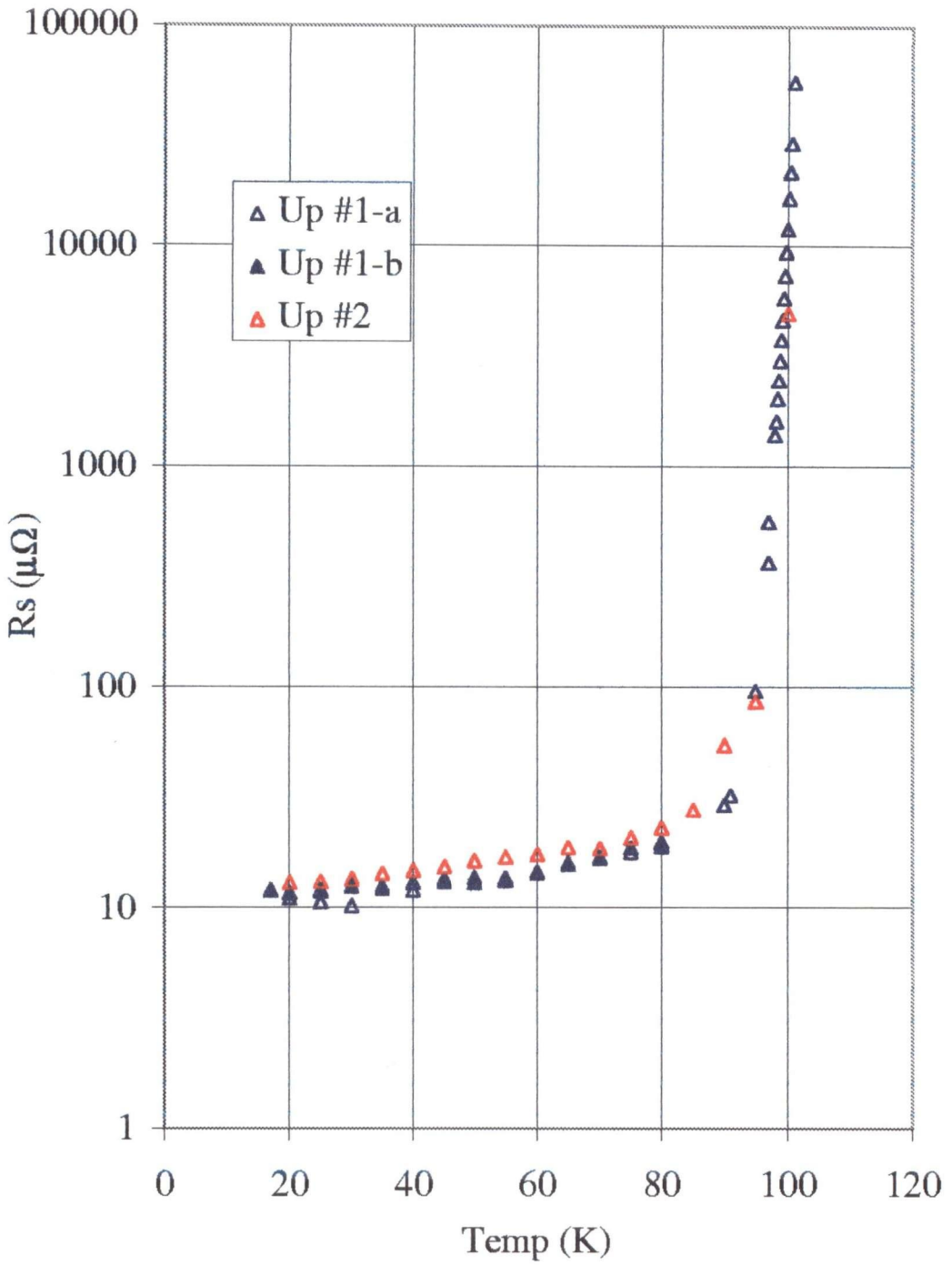

Figure 5.25: R_S for all samples at 2.4 GHz – Semi-Log Plot

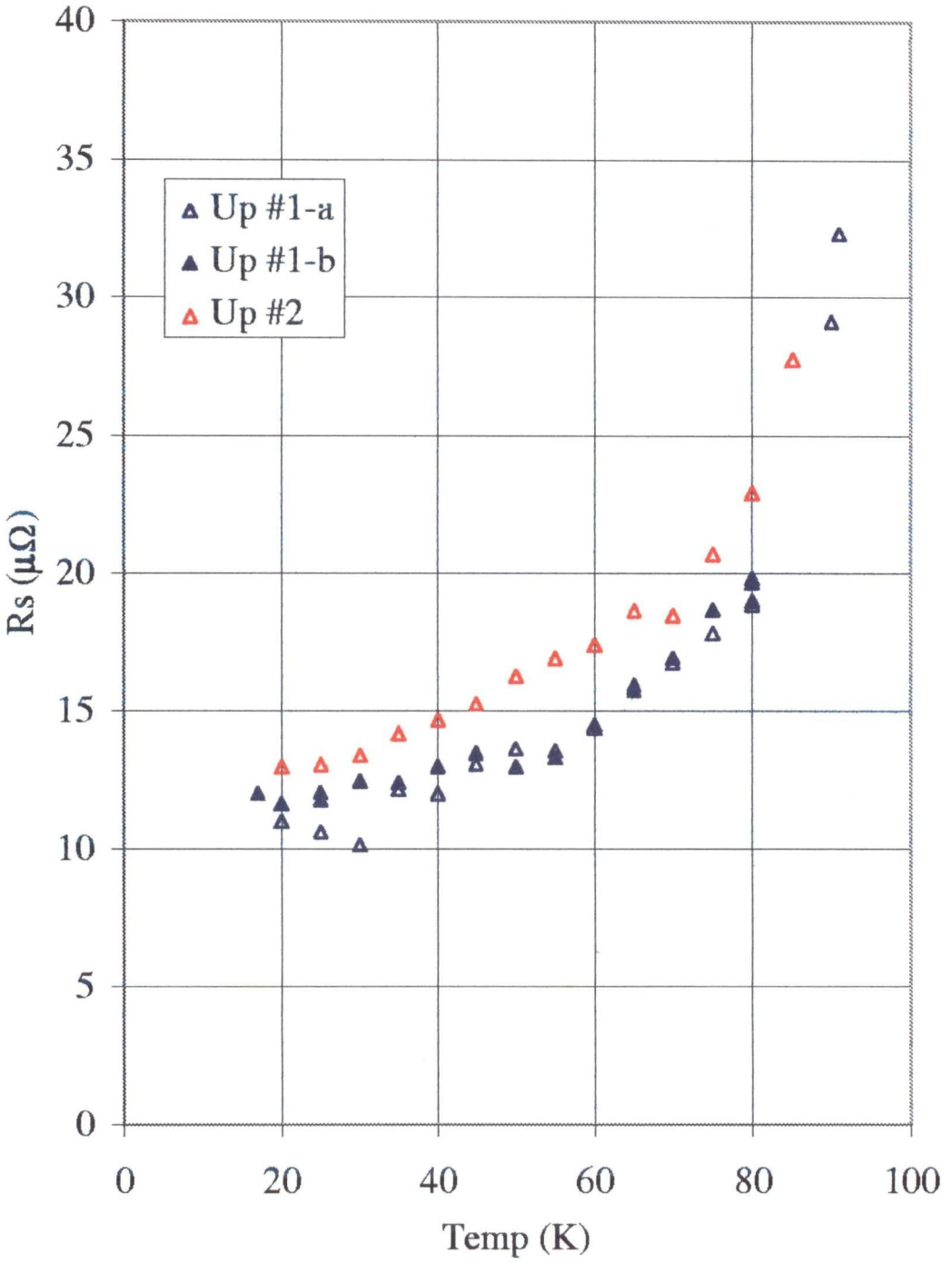

Figure 5.26: R_S for all samples at 2.4 GHz – Linear Plot

5.1.4 Results at 3.7 MHz

The 3.7 GHz measurements were performed with the previous resonator[1].

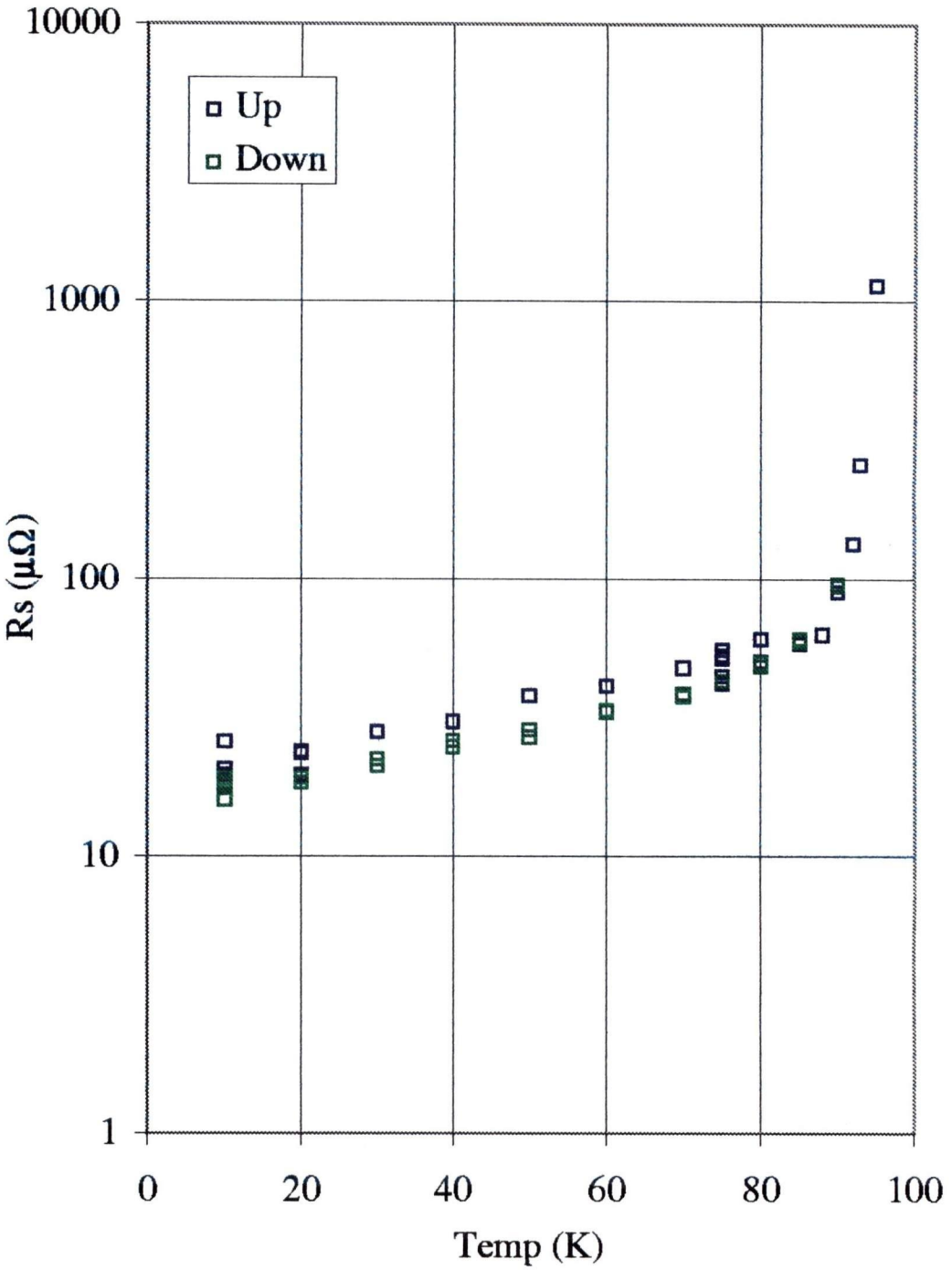

Figure 5.27: R_S for all samples at 3.7 GHz – Semi-Log Plot

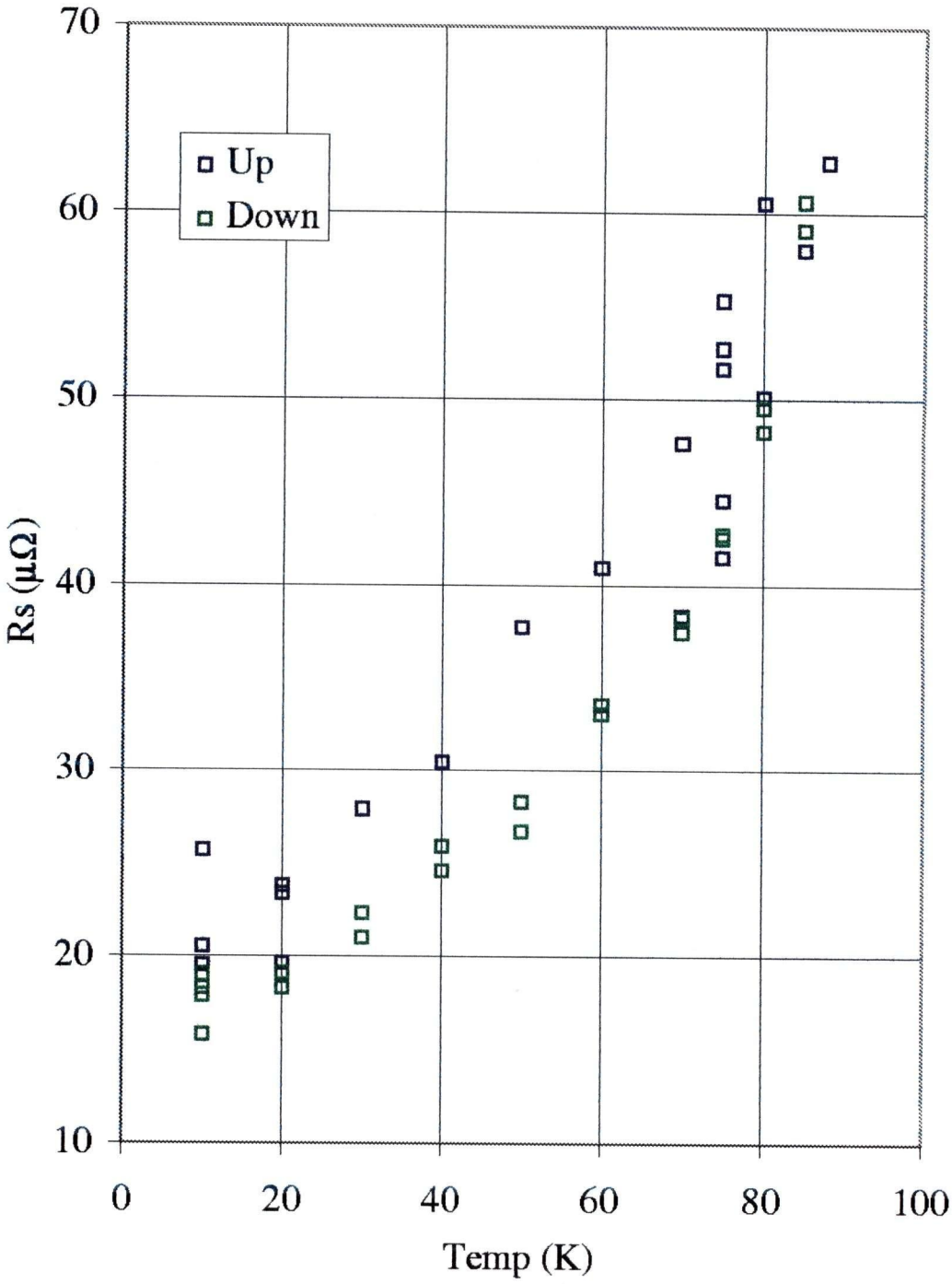

Figure 5.28: R_S for all samples at 3.7 GHz – Linear Plot

Date	Sample	Frequency (GHz)	$Q_O x 10^6$	$R_S(min)$	$R_S(77K)$
Aug 14, 1997	Up 1	0.91	1.7	3	5
July 18, 1997	Up 1	1.4	3.5	10	14
Mar 15, 1997	Up 1	2.4	5.5	12	19
Jan 19, 1997	Up	3.7	1.9	20	45
Aug 13b, 1997	Up 2	0.91	1.8	3	4
July 17, 1997	Up 2	1.4	4.0	6	8
April 10, 1997	Up 2	2.4	2.1	13	21
Aug 15, 1997	Down 3	0.91	1.3	5	6
June 23, 1997	Down 3	1.4	4.2	5	8
Feb 1, 1997	Down	3.7	2.0	16	43
Aug 13, 1997	Down 4	0.91	1.7	3	4
Aug 11, 1997	Down 4	1.4	4.0	6	10

Table 5.8: List of all Surface Resistance Measurements

5.1.5 Summary of All Results

From figures 5.29 & 5.30, it can be seen that all four samples, regardless of "Up" or "Down" in their origin, demonstrate similar losses and transition temperatures. It is not surprising that the losses differ widely at different frequencies. What is interesting, however, is the fact that the temperature dependence of the losses differs qualitatively at different frequencies and does not follow ω^2 scaling, as discussed in the remaining section.

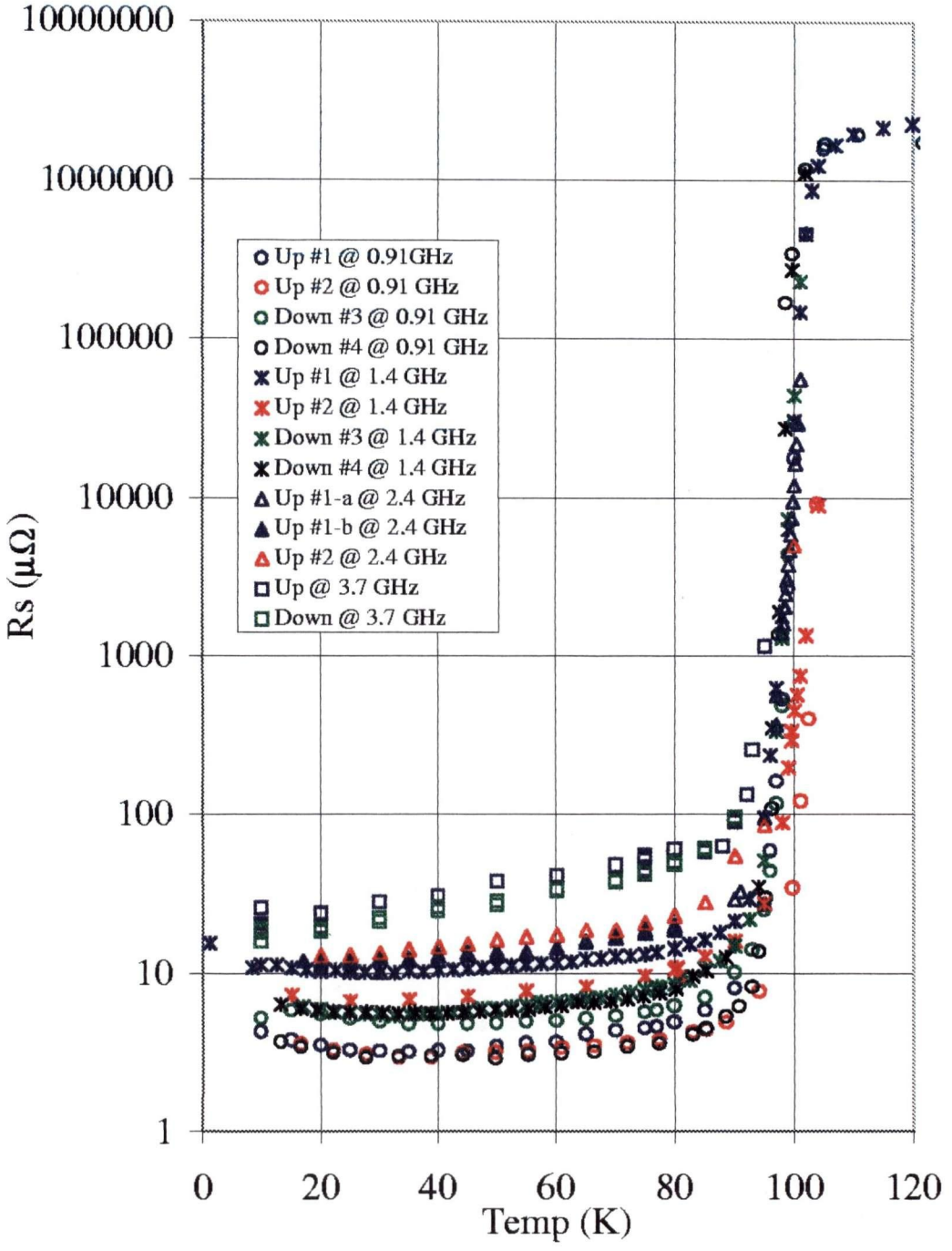

Figure 5.29: R_S for all Samples , 0–120K Semi-Log Plot

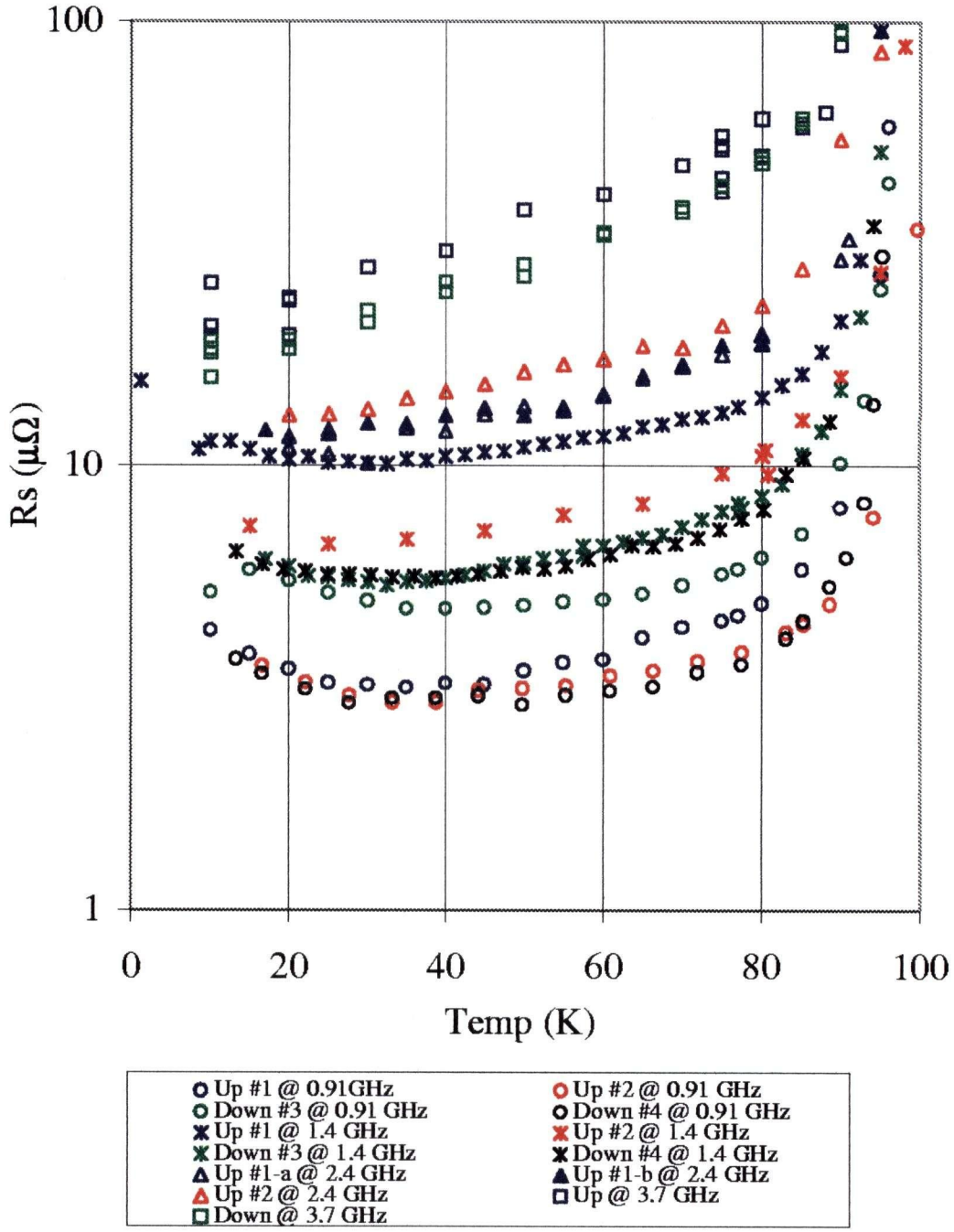

Figure 5.30: R_S for all Samples, 0–100K Semi-Log Plot

5.2 Frequency Dependence

With the intended operation of these films being at 1 GHz, and with the ability of existing techniques restricted to higher frequencies for measurements on such low loss films, the question of the appropriateness of ω^2 scaling of data can now be addressed.

If ω^2 scaling is valid for such films, then scaling all of the results to an arbitrarily decided frequency should produce results that all have the same shape and absolute size. Here the data has been scaled up to 3.7 GHz. Due to the fact that the Up #1 and Down #3 samples both have runs with results that are in question, only the remaining two samples are used for this calculation. Unfortunately, for the 3.7 GHz results, it is not known for sure if the "Up" and "Down" measurements are in fact #2 and #4 respectively. They have though, still been included since there do not appear to be large differences in the results of each pair of samples in each group.

Figure 5.32 clearly demonstrates differences in both the absolute size and the shape of the temperature dependence of the results for both samples. This is particularly evident at lower temperatures. The non ω^2 behaviour is more clearly seen if one examines the explicit frequency dependence at various temperatures. Figures 5.33, 5.34, and 5.35 show this dependence at temperatures of 20 K, 70 K, and 80 K respectively. The solid lines included are proportional to ω^2. Figure 5.36 shows the data of figure 5.33 graphed as a function of the square of frequency. From the least squares fit shown in the figure, it is clear that the zero frequency intercept is non zero and is, in fact, near $3.1\mu\Omega$. Once again, it is at the lower temperatures where the deviation from ω^2 dependence is evident. Discussion of potential causes for this behaviour is the topic of the final chapter.

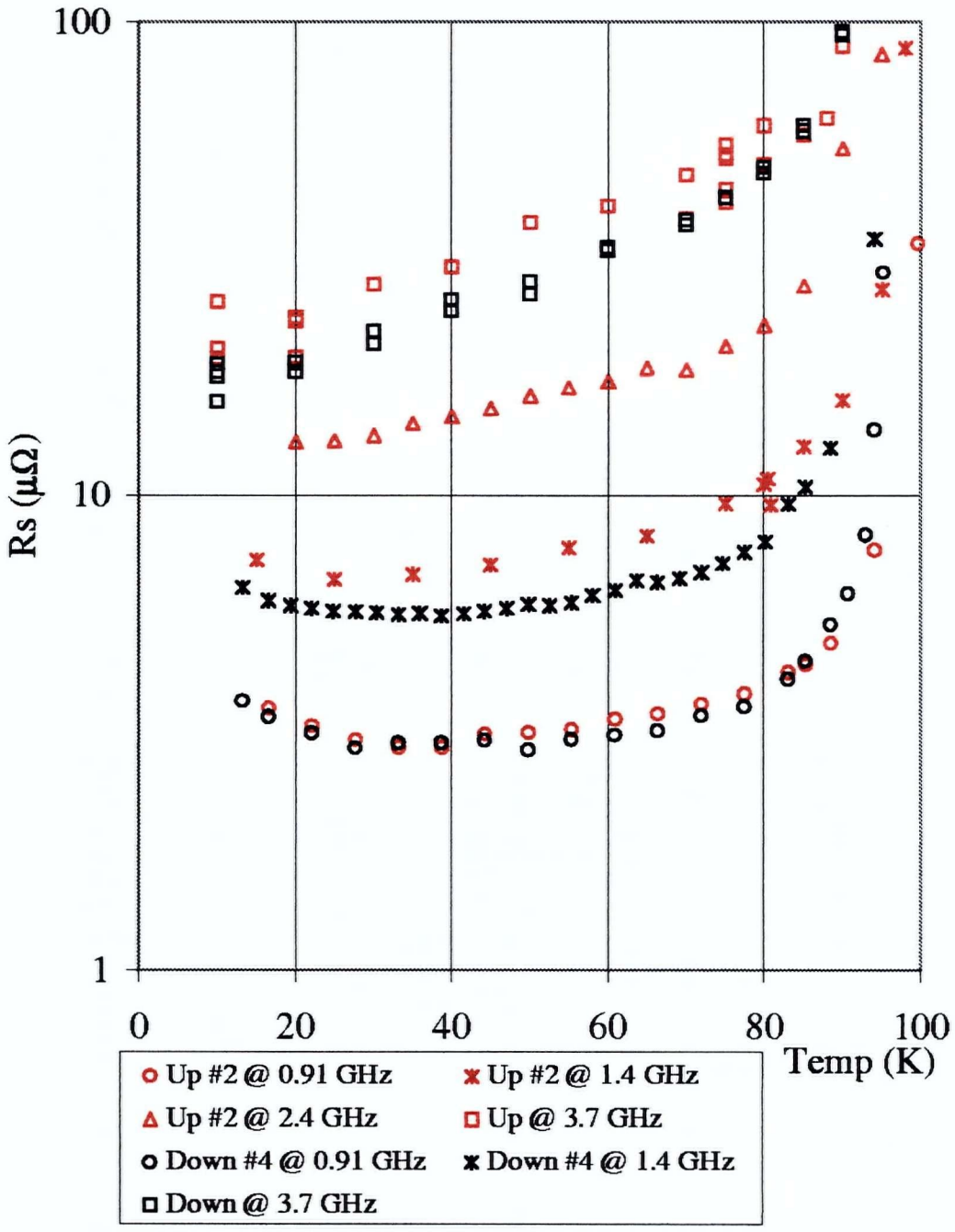

Figure 5.31: Unscaled Results for Samples #2 and #4

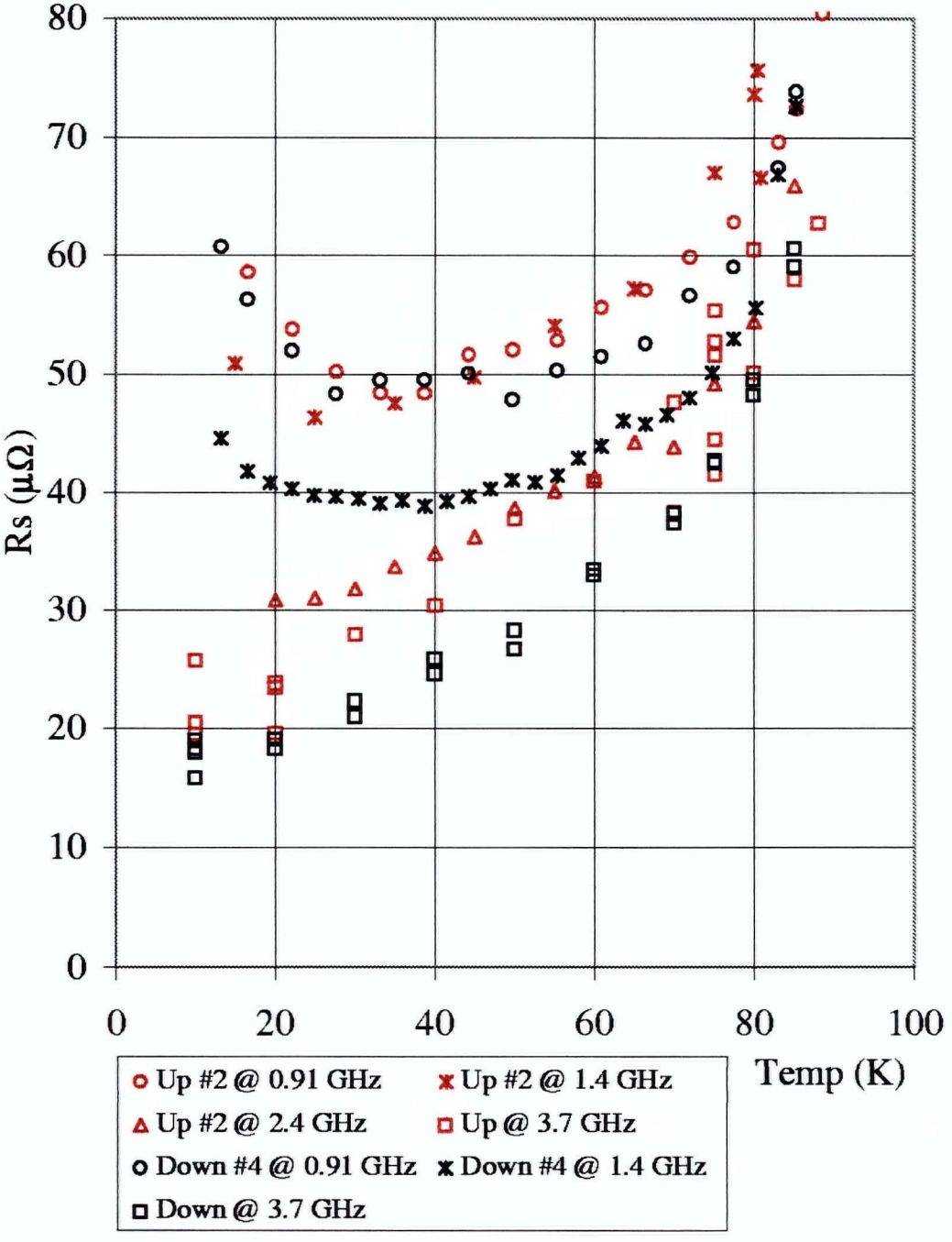

Figure 5.32: ω^2 Scaled Results for Samples #2 and #4

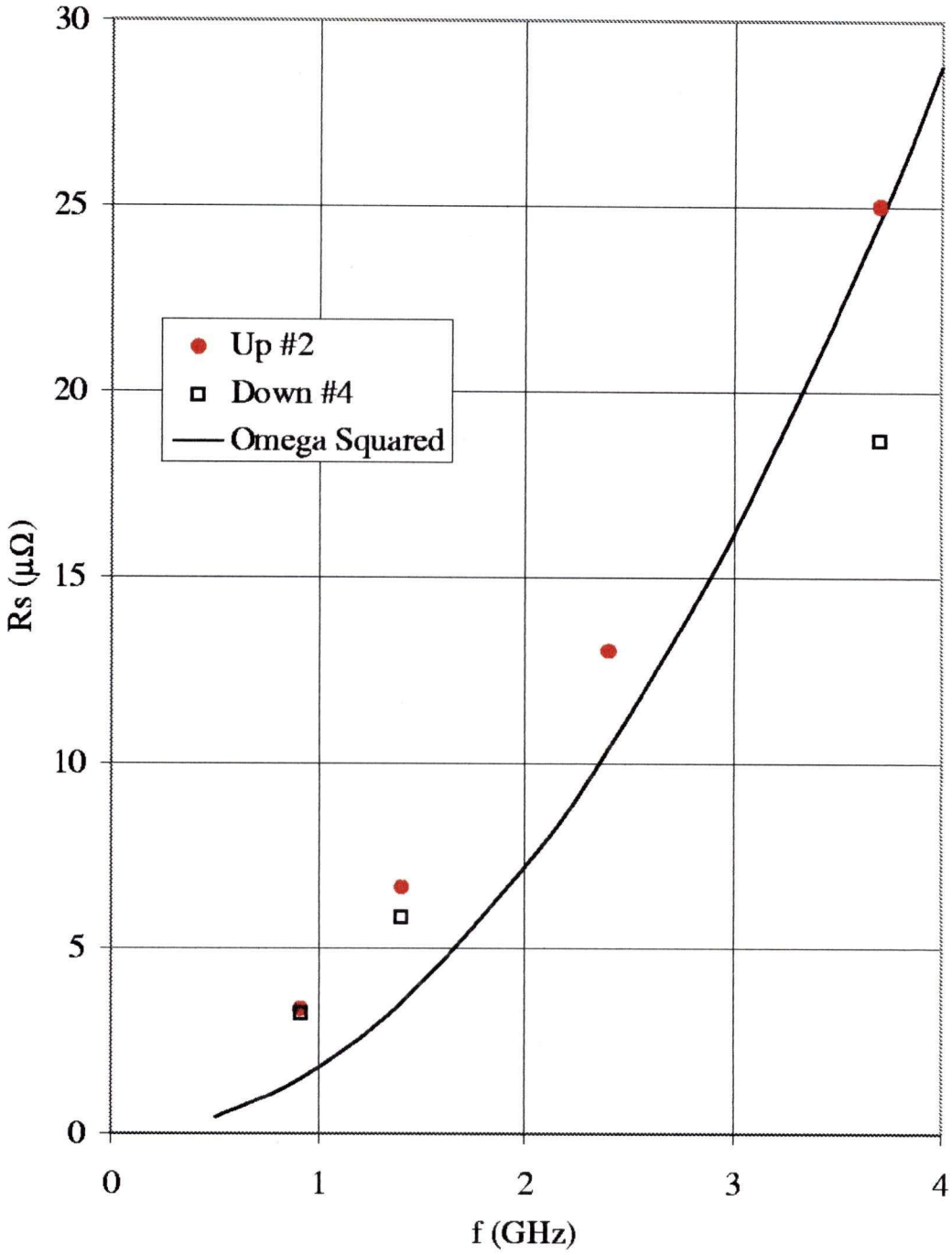

Figure 5.33: Frequency dependence of R_S at 20K. The solid line is proportional to ω^2.

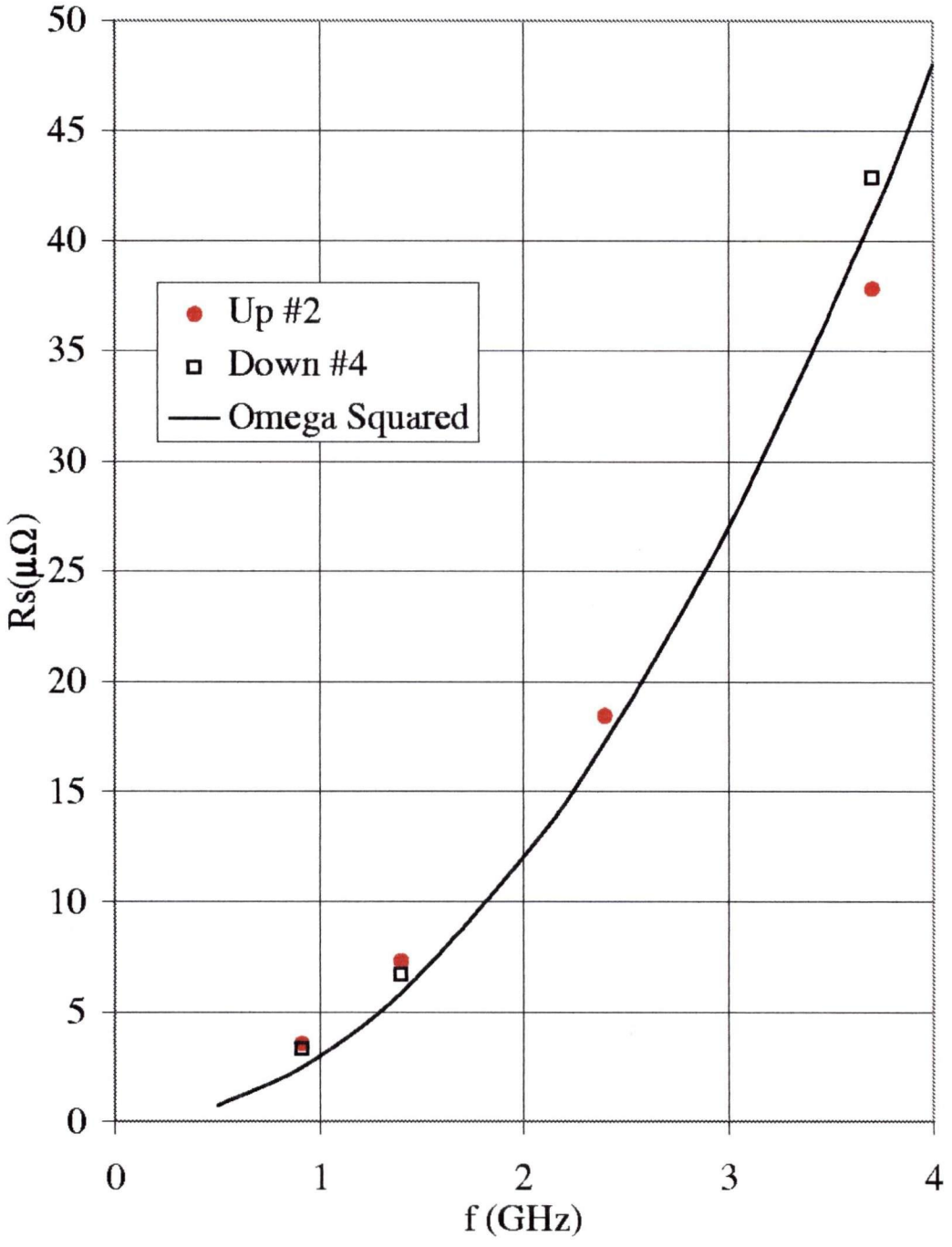

Figure 5.34: Frequency dependence of R_S at 70K. The solid line is proportional to ω^2.

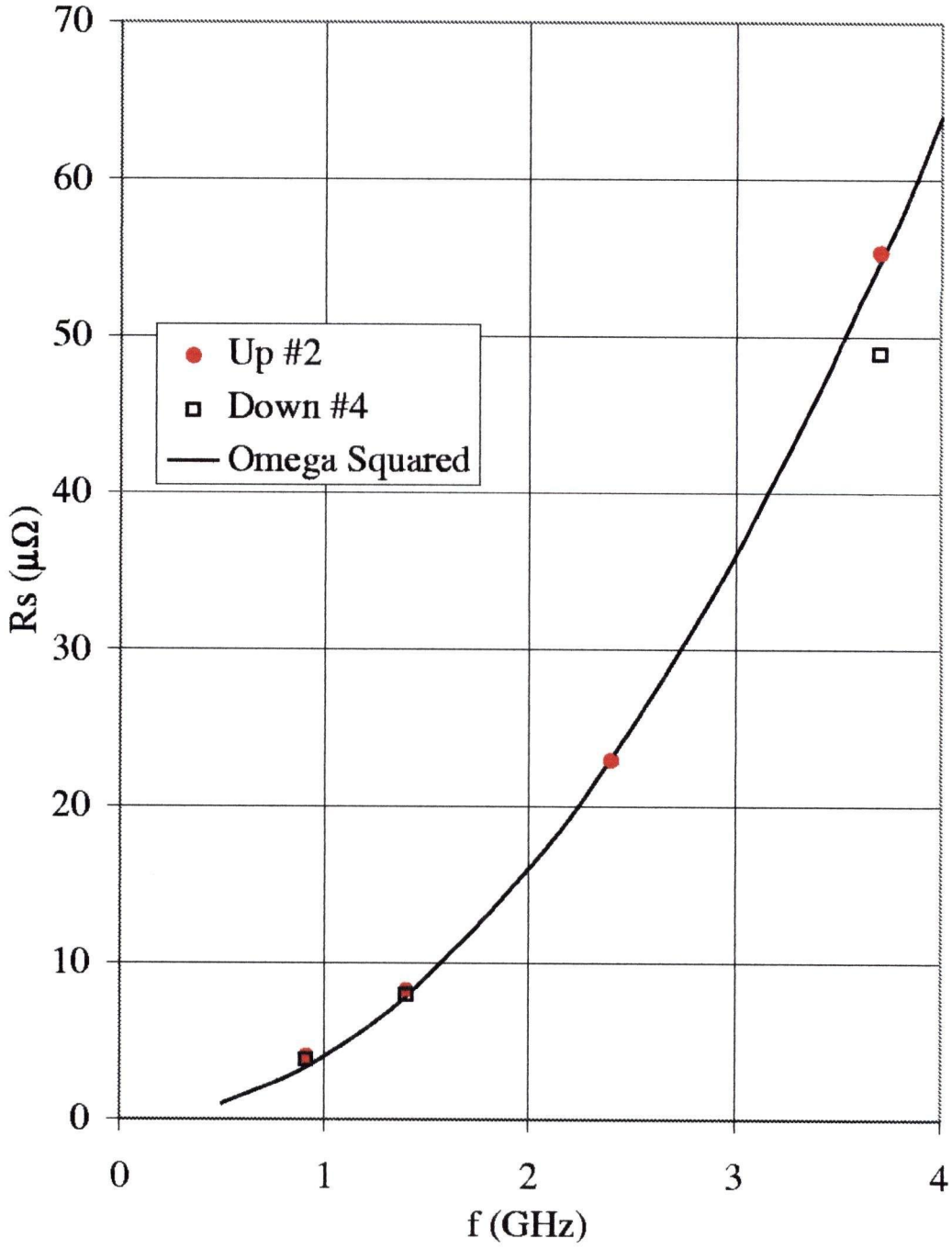

Figure 5.35: Frequency dependence of R_S at 80K. The solid line is proportional to ω^2.

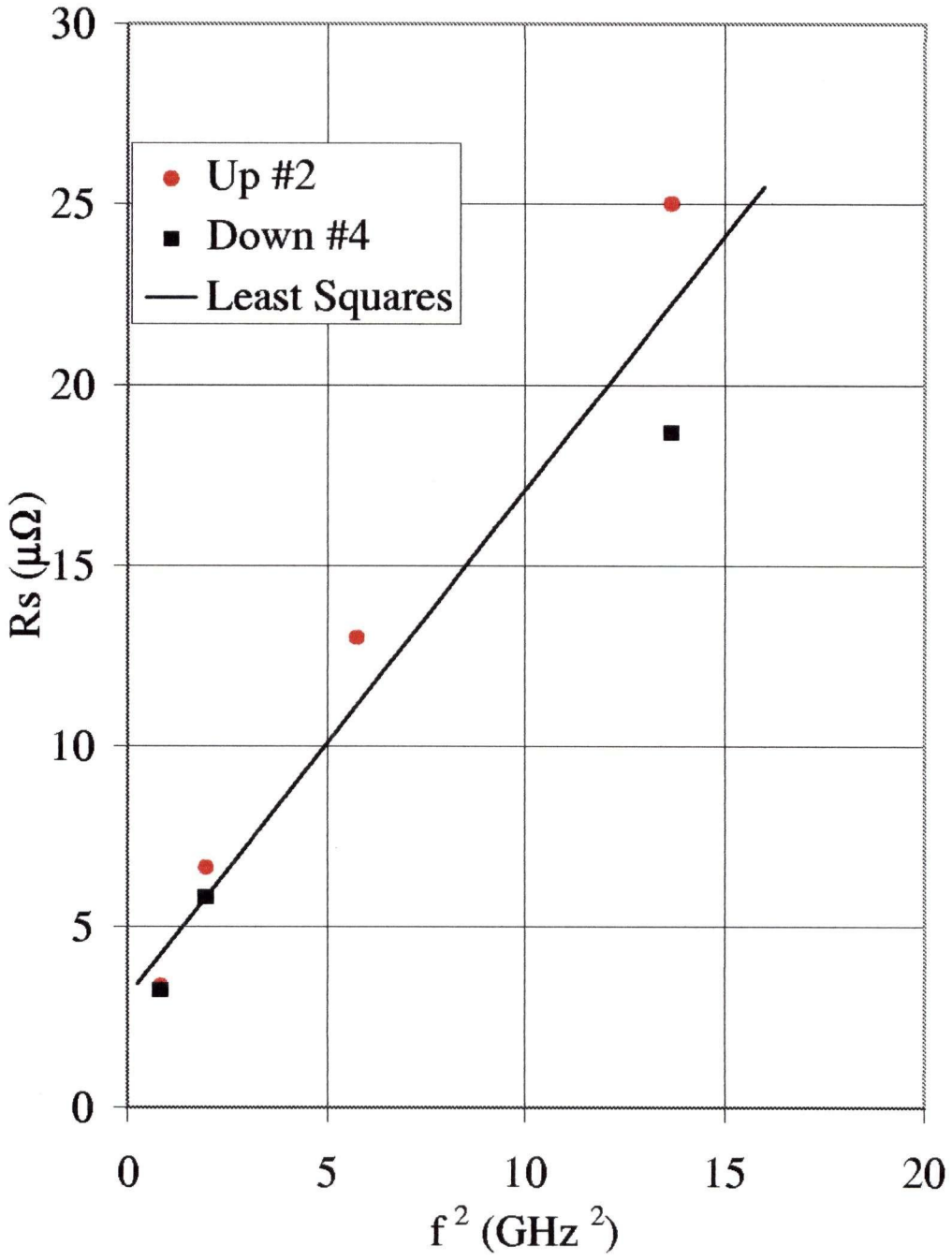

Figure 5.36: Frequency dependence of R_S at 20K graphed as a function of frequency squared. The intercept of the least squares fit is near $3.1\mu\Omega$.

Chapter 6

Discussion and Conclusions

6.1 Performance of the Resonator

The improvements in the new design of the resonator and the intrinsic power in general of split-ring resonators to resolve losses in small high quality samples demonstrate that this measurement platform is sufficient to keep pace with the latest demands of the newest films available.

The Pb:Sn surface is simpler than niobium to prepare and does not show signs of degrading with time in atmosphere. In fact, during a 2 month period of time during the 1.4 GHz measurements, the unloaded quality factor did not measurably decrease.

The sapphire support arrangement causes no microphonics at the resonator itself and eliminates the troubles of $\lambda/4$ resonances interfering with the resonance of the ring. The elimination of superconducting joints in the resonator ensures high unloaded quality factors relatively free of power dependence problems.

Finally, the ability to quickly re-tune the resonator by switching ring sets and gap thicknesses provides a valuable tool for performing microwave loss measurements at frequencies equal to that of the intended application and to study frequency dependence.

6.1.1 Potential Improvements to Follow

Potentially, the resonator's resolution power and ease of operation could still see some improvement. Better thermal contact between the "core" and the helium bath would

Frequency (GHz)	Temp (K)	R_S	Method
9.6	77	200 $\mu\Omega$	Nb Cavity Perturbation [13]
9.6	90	400 $\mu\Omega$	
10	4.2	23 $\mu\Omega$	Parallel Plate [14]
10	77	130 $\mu\Omega$	
20	104	18 mΩ	Parallel Plate[14]
5.6	77	61 $\mu\Omega$	Dielectric Resonator[15]
27.5	4.2	212 $\mu\Omega$	Dielectric Resonator[15]
94	77	13.6 mΩ	Confocal Resonator[15]

Table 6.9: Previous Measurements of $Tl_2Ba_2CaCu_2O_y$ Thin Films

provide a more stable unloaded quality factor thus making measurements of the lowest losses more reliable. Although not as stable in air, the niobium ring set may have potential in increasing the unloaded quality factor. Due to the problems with degradation of the niobium surface, the desire to use niobium also motivates the development of a top loading sample air-lock to allow switching samples without warming the resonator and exposing it to atmosphere.

6.2 Performance of the $Tl_2Ba_2CaCu_2O_y$ Films

All four of the $Tl_2Ba_2CaCu_2O_y$ films have proven to show very low microwave loss consistent with previous measurements made on similar films also from STI. Some of the existing surface resistance measurements are shown in table 6.9 including the method of employed. With losses in the order of a few micro-ohms at 1 GHz and Liquid Nitrogen temperatures, they are ~500 times better than that of OFHC copper and only one order of magnitude from typical residual losses exhibited by Pb:Sn[12] compounds at 1K! Just as impressive is the ability of the new split-ring resonator to now measure the low values of R_s that are demonstrated by the films at this 1 GHz frequency range.

6.2.1 ω^2 Frequency Dependence

The ω^2 scaled results shown in figures 5.32 and the frequency dependence shown in figures 5.33, 5.34, 5.35 and most importantly 5.36, clearly demonstrate that the microwave losses of these $Tl_2Ba_2CaCu_2O_y$ films do not scale with the square of frequency at low temperatures. This is evident in the larger than expected absolute size of the losses for both measurements below 2 GHz. In addition to demonstrating an absolute residual loss that becomes significant below 2 GHz, the shape of the temperature dependence curve is also quite different at the lower frequencies. Measurements above 2 GHz show losses that continue to decrease with decreasing temperature. The lower frequencies, however, demonstrate first a flattening around 1.4 GHz and then a clear upturn at lower temperatures at 910 MHz. The previously recorded measurements of the $Tl_2Ba_2CaCu_2O_y$ films[13][14][15] have shown that in the 5–95 GHz range, R_s does scale with ω^2. Adding the previous data, scaled to 3.7 GHz, to figure 5.32 one finds the 3.7 GHz data only slightly higher than the previous results. It is then apparent that the ω^2 frequency dependence breaks down for frequencies below ~2–3 GHz. Below these frequencies, which corresponds to an energy scale of ~0.1 K, the temperature dependence of R_s begins to adopt a $\sim T^{-1}$ form. This is not at all unlike the lower frequency temperature dependence of $YBa_2Cu_3O_{6.95}$ single crystals doped with Zinc impurities at the 0.3% level: for such samples, R_s at 35 GHz[16] does not demonstrate the upturn at low temperatures; for measurements at 3.7 GHz[17], on the other hand, R_s experiences a dramatic upturn below 10 K. In the case of zinc doped $YBa_2Cu_3O_{6.95}$, the low temperature upturn may perhaps be described by considering the spin zero Zn atoms as magnetic impurities within the $YBa_2Cu_3O_{6.95}$ lattice of spin 1/2 Cu sites. The addition of the Zn atoms, which themselves are not magnetic, then creates a complex permeability to the lattice

given by,

$$\mu = \mu_0(1 + \chi' - i\,\chi''). \tag{6.39}$$

The surface impedance then becomes,

$$Z_S = \left(\frac{i\mu_0(1 + \chi' - i\,\chi'')\omega}{\sigma_1 - i\,\sigma_2}\right)^{1/2}. \tag{6.40}$$

With the assumptions of $\chi << 1$ and $\sigma_2 >> \sigma_1$ the real part of equation 6.40 can be shown[18] to yield,

$$R_S = \mu_0^2\omega^2\lambda^3(\sigma_1 + \sigma_2\chi'') \tag{6.41}$$

for R_s in the presence of trace impurities. Interestingly, σ_2, which is much larger than σ_1 for a superconductor, is proportional to $(\omega\lambda^2)^{-1}$, and can therefore allow the small value of χ'' for these doping concentrations to become noticeable at lower frequencies.

In the case of the $Tl_2Ba_2CaCu_2O_y$ samples, it is also conceivable that a similar magnetic impurity situation could be created during the growth of the film. This idea is strongly supported by the increasing presence of the low temperature up turn as one moves to lower frequencies.

The ability to perform temperature dependent measurements on low loss superconducting films at these low and varied frequencies is further testament to the resolution power and frequency flexibility of this new form of split-ring measurement.

Bibliography

[1] D.A. Bonn, D.C. Morgan, and W.N. Hardy. Split- Ring Resonators for Measuring Microwave Surface Resistance of Oxide Superconductors, *Rev. Sci. Instr.*, **62**, 1819, 1991.

[2] G.L. Matthaei, G.L. Hey-Shipton. Novel Staggered Resonator Array Superconducting 2.3 GHz Bandpass Filter, *IEEE Trans on Microwave Theory and Techniques*, **41**, 2345, 1993.

[3] D.A. Bonn and W.N. Hardy, in *Physical Properties of High Temperature Superconductors*, edited by Donald Ginsberg (World Scientific, Singapore, 1996) vol. VI, p. 7.

[4] M.A. Allen, Z.D. Farkas, H.A. Hogg, E.W. Hoyt and P.B. Wilson. Superconducting Niobium Cavity Measurements at SLAC, *IEEE Proc. Appl. Superconductivity Conf.*, **72**, 621, 1972.

[5] J.M. Pierce, H.A. Schettman, W.M. Fairbank, and P.B.Wilson. RF Losses in Superconducting Lead and Niobium, *Proc. Int. Conf. on Low Temp. Phys*, **A**, 396, 1964.

[6] Z.Y. Shen, C. Wilker, P. Pang, W.L. Holstein, and D. Face. High Tc Superconducting Sapphire Microwave Resonator with Extremely High Q Values Up to 90 K, *IEEE Trans. on Microwave Theory and Techniques*, **40**, 2424, 1992.

[7] W.K. Hui, and I. Wolff. Dielectric Ring Gap Resonator for Application in MMIC's, *IEEE Trans. on Microwave Theory*, **39**, 2061, 1991.

[8] J.R. Delayen, C.L. Bohn, and C.T. Roche. Apparatus for Measurement of Surface Resistance Versus RF Magnetic Field of High-Tc Superconductors, *Rev. Sci. Instr.*, **61**, 2207, 1990.

[9] W.N. Hardy and L.A. Whitehead. Split-Ring Resonator for use in Magnetic Resonance from 200-2000 MHz, *Rev. Sci. Instr.*, 52, 213, 1981.

[10] G. Schaumburg and H.W. Helberg, Application of a Cavity Perturbation Method to the Measurement of the Complex Microwave Impedance of Thin Super or Normal Conducting Films, *Journal de Physique III*, **4**, 917, 1994.

[11] A.W. Kraszewski and S.O. Nelson. Resonant Cavity Perturbation - Some New Applications of an Old Technique, *Journal of Microwave Power and Electromagnetic Energy*, **31**, 178, 1996.

[12] L. Dietl and U. Trinks. The Surface Resistance of a Superconducting Lead-Tin Alloy, *Nucl. Instrum.*, **A284**, 283, 1989.

[13] R.B. Hammond, G.V. Negrete, L.C. Bourne, D.D. Strother, A.H. Cardona, and M.M. Eddy, Epitaxial $Tl_2CaBa_2Cu_2O_8$ Thin Films with Low 9.6 GHz Surface Resistance at High Power above 77 K, *Appl. Phys. Lett.*, **57**, 825, 1990.

[14] W.L. Holstein, L.A. Parisi, Z.Y. Shen, C.Wilker, M.S. Brenner, and J.S. Martens. Surface Resistance of Large Area $Tl_2Ba_2CaCu_2O_8$ Thin Films at Microwave and Millimeter Wave Frequencies Measured by Three Noncavity Techniques, *Journal of Superconductivity*, **6**, 191, 1993.

[15] W.L. Holstein, L.A. Parisi, C. Wilker and R.B. Flippen. $Tl_2Ba_2CaCu_2O_8$ Films with Very Low Microwave Surface Resistance up to 95 K, *Appl. Phys. Lett.*, **60**, 2014, 1993.

[16] D.A Bonn et al., *Phys. Rev. B*, **50**, 4051, 1994.

[17] D.A. Bonn, S. Kamal, A. Bonakdarpour, R. Liang, W.N. Hardy, C.C. Homes, D.N. Basov, and T. Timisk. Surface Impedance Studies of YBCO, *Proc. of the 21st Int. Conf on Low Temp. Phys.*, **46**, 3195, 1996.

[18] D.A. Bonn, A.J. Berlinsky. Private Communication.

[19] *A Compendium of the Properties of Materials at Low Temperature*, National Bureau of Standards Cryogenic Engineering Laboratory, Boulder Colorado, Dec. 1961.

Appendix A

Resistivity of Lead

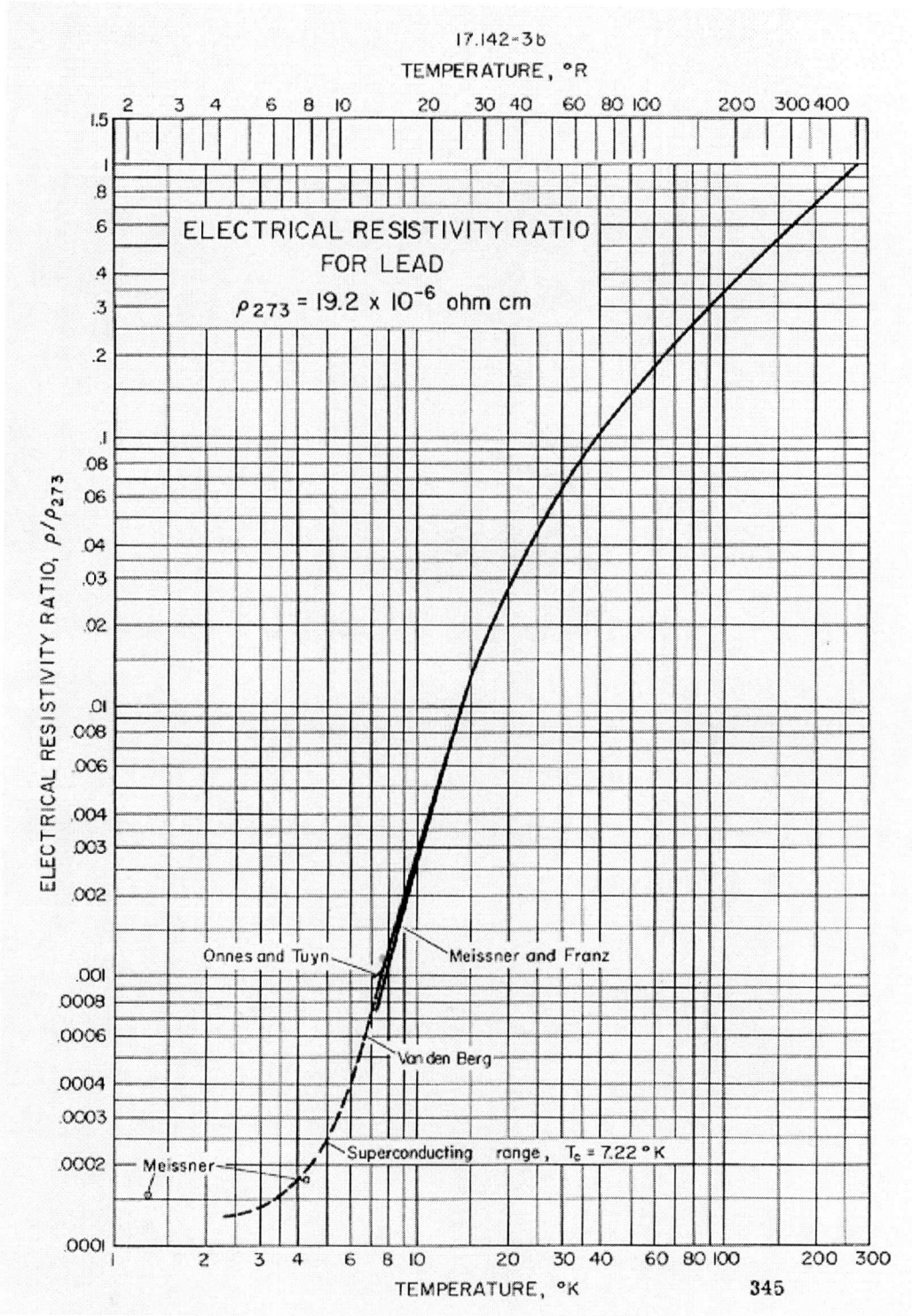

Figure A.37: DC Resistivity of Lead[19]

Appendix B

Detailed Plans for the Resonator

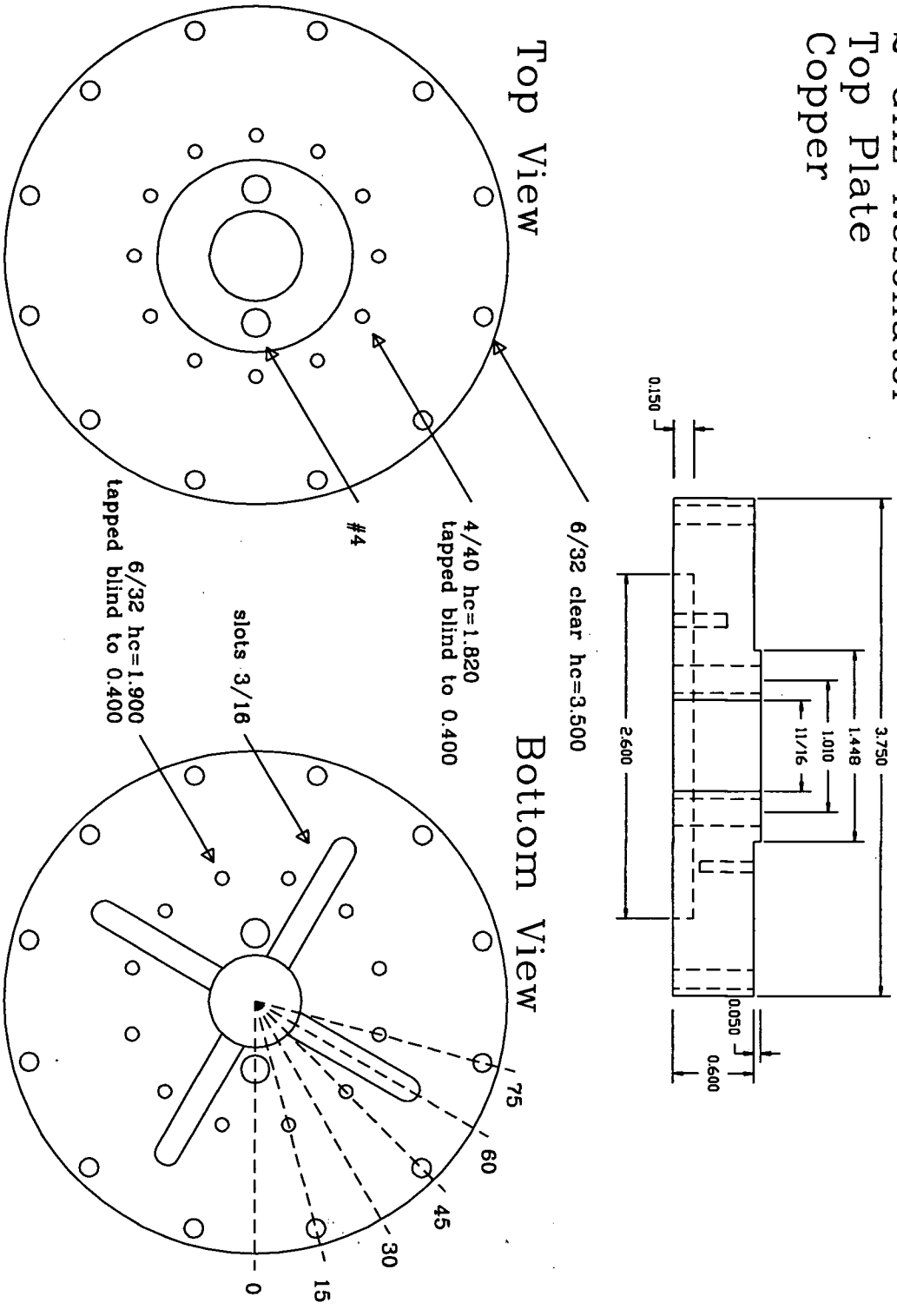

Figure B.38: Resonator Top Plate

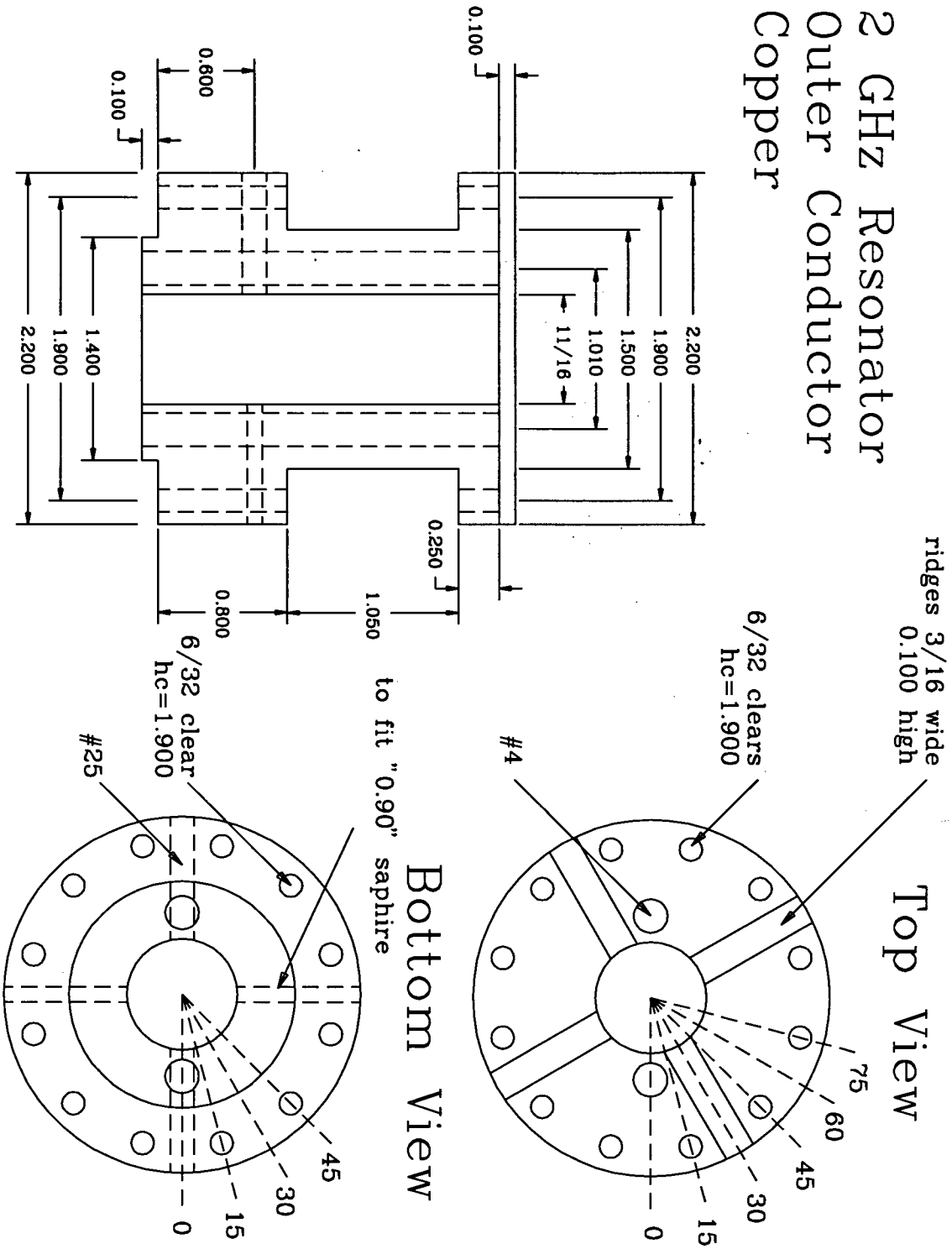

Figure B.39: Resonator Core

2 GHz Resonator
Bottom Cap
Copper

Top View

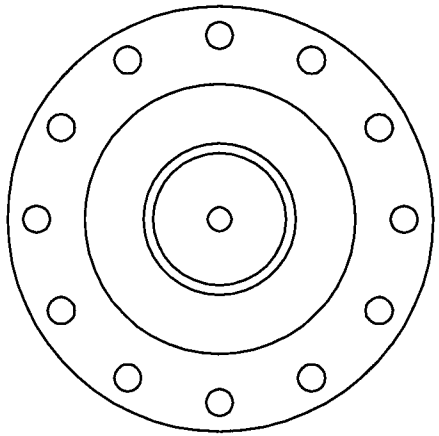

Bottom View

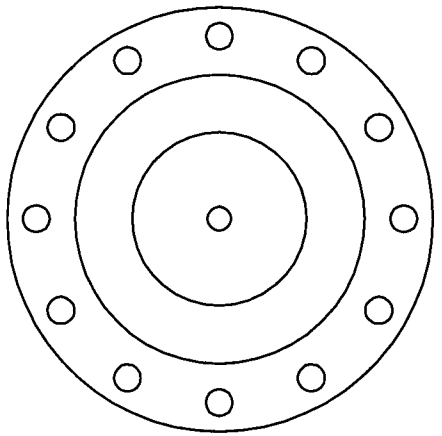

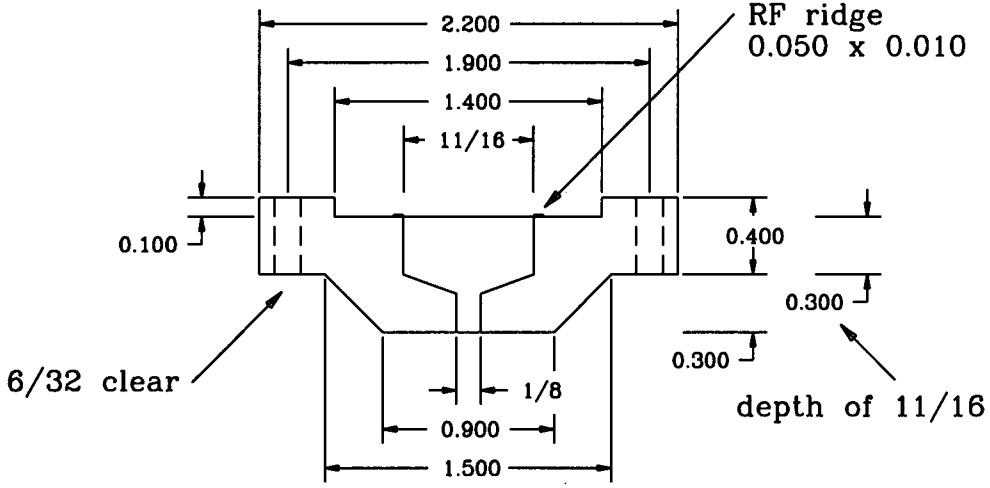

Figure B.40: Resonator Bottom Cap

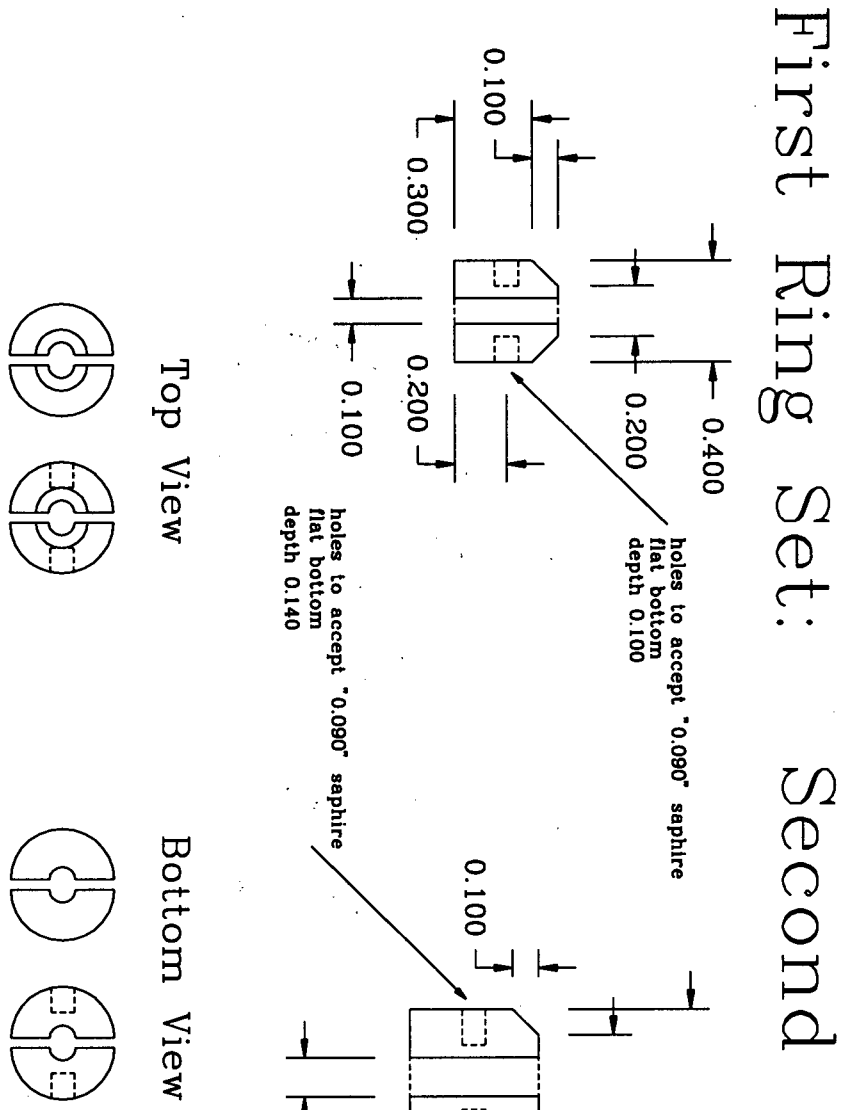

Figure B.41: Resonator Ring Sets